

NASA-TM-107,002

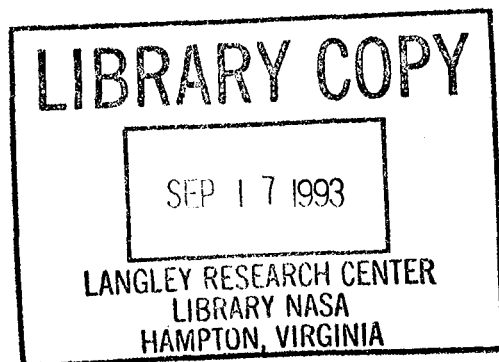
NASA Technical Memorandum 109002

NASA-TM-109002 19940008338

24 GHz Measurements of 2.2 Lambda Conical Horn Antennas Illuminating a Conducting Sheet

A. E. Cross, R. E. Marshall, C. P. Hearn, and
R. T. Neece

June 1993



NASA

National Aeronautics and
Space Administration

Langley Research Center
Hampton, Virginia 23681-0001

TABLE OF CONTENTS

Symbols and Abbreviations	ii
1.0 Summary	1
2.0 Introduction	2
2.1 Background	2
2.2 MRIS	2
2.3 Present Work	3
3.0 Experimental System Configuration	4
3.1 Reflectometer and Measurement Circuit	5
3.2 Antennas	6
3.3 Ground Plane and Reflecting plate	6
3.4 Thermal Protection System (TPS) Tiles	8
3.5 Plate Positioning System	9
4.0 Experimental Measurements and Discussion	10
4.1 Range Measurements	10
4.1.1 With Ground Plane, Without TPS Tile	10
4.1.2 With Ground Plane, With TPS Tile	12
4.1.3 Without Ground Plane, Without TPS Tile	13
4.1.4 Without Ground Plane, With TPS Tile	14
4.2 Tilt Measurements	15
4.2.1 With Ground Plane, Without TPS Tile	15
4.2.2 With Ground Plane, With TPS Tile	16
4.2.3 Without Ground Plane, Without TPS Tile	16
4.2.4 Without Ground Plane, With TPS Tile	17
5.0 Theoretical Models and Comparison with Experimental Results	17
6.0 Conclusions	19
7.0 References	21

Symbols and Abbreviations

AFE	Aeroassist Flight Experiment
CFD	computational fluid dynamics
CW	continuous wave
CWG	circular waveguide
d	distance between aperture plane and reflecting plate, cm
D	diameter of antenna aperture, cm
D_a	diameter of conical horn aperture, cm
D_e	effective diameter of conical horn aperture on ground plane, cm
dB	decibel
FF	far-field range ($d = 2D^2/\lambda$), cm
GEO	geosynchronous Earth orbit
GHz	gigahertz
LEO	low Earth orbit
L	attenuation loss, dB
MRIS	Microwave Reflectometer Ionization Sensor
NASA	National Aeronautics and Space Administration
P _f	forward power in directional coupler, dB
P _r	reverse power in directional coupler, dB
RAM	Radio Attenuation Measurements experiments
RCG	reaction cured glass
RF	radio-frequency
STS	Space Transportation System
TPS	thermal protection system
$ \Gamma $	magnitude of the power reflection-coefficient, dB
ϕ	aperture phase deviation, deg.
λ	wavelength at 24 GHz (1.249 cm)

1.0 Summary

Monostatic reflection-coefficient magnitude, $|\Gamma|$, measurements occurring between a radiating horn and a metal (aluminum) reflecting plate are presented for three 2.2λ diameter conical horn antennas. The variable element between the three horns is the aperture phase deviation, which varies from 6° to 125° . Measurements of $|\Gamma|$ as a function of horn-plate separation distance (or range) extend from an antenna aperture short ($d = 0$) to beyond the far-field boundary ($d = 2D^2/\lambda$), where D is the antenna diameter. Comparative measurement data are presented with varying intermediate physical environments for each of the horns. These physical environments are horn antenna with and without the use of a ground plane, with and without an intermediate dielectric material covering the horn aperture, and with varying angles of tilt for the metal plate.

The measured scalar data from the conical horns with various aperture phase deviations, mounted on finite ground planes, are compared with data from a theoretical model that uses a circular waveguide aperture with zero phase deviation mounted on an infinite ground plane. The measured scalar data from the conical horns, with and without the use of a ground plane, are also compared to a scalar diffraction theory model.

This work was performed in support of an effort to develop a multifrequency microwave reflectometer, to be flown on a space vehicle, that would accurately determine the distance from the vehicle surface to a reflecting plasma boundary. A metal reflecting plate was used in this work to simulate RF reflectivity from a critically dense plasma. This resulted in a strong interaction between the ground plane mounted aperture and the reflecting plate at integral half-wavelength separations for a variety of test conditions.

2.0 Introduction

2.1 Background

The Aeroassist Flight Experiment (AFE) was a National Aeronautics and Space Administration (NASA) research program to investigate and validate atmospheric braking for a spacecraft returning to the Earth's atmosphere. The AFE spacecraft would be placed in orbit from the Space Transportation System (STS) and then accelerated to reenter the Earth's atmosphere at geosynchronous Earth orbit (GEO) return velocities. The AFE spacecraft would then use the atmosphere for aerodynamic braking in order to obtain low Earth orbit (LEO) velocities. To improve future aerobrake design, accurate heating rate data would have to be collected during the AFE aerobraking maneuvers. A series of onboard experiments were proposed and selected to aid in the validation of the most current computational fluid dynamics (CFD) codes that are used to predict stagnation region heating rates for all reentry spacecraft, including aerobrakes.

2.2 MRIS

The Microwave Reflectometer Ionization Sensor (MRIS) was one of the AFE experiments. Previous experience (ref. 1) using continuous wave (CW) microwave reflectometers during successful reentry plasma diagnostic flight experiments on the Radio Attenuation Measurement (RAM) series of vehicles was the basis for the MRIS proposed experiment. The total flight regime for the AFE spacecraft, however, would impose more severe flight and measurement constraints upon the MRIS than were imposed upon the RAM reflectometer instrument. The MRIS was a four-frequency, stepped-frequency millimeter wave reflectometer instrument with sensor antennas located under the Thermal Protection System (TPS) tile in the AFE vehicle's stagnation region. The four center-frequencies were 20, 44, 95, and 140 GHz, with frequency stepping occurring over a 4 GHz bandwidth for each center frequency. The MRIS instrument's purpose was to measure, as a function of frequency and aerobrake trajectory, the distance to the critical electron density from the vehicle's surface and the magnitude of the reflection from the critical electron density. In parallel with the

development of the MRIS instrument, an ongoing series of experimental laboratory studies were conducted to investigate potential problem areas for the instrument and to provide confidence in the performance characteristics of the flight-instrument configuration.

2.3 Present Work

Experimental laboratory studies were initially made in 1988 during a feasibility study to demonstrate the ability to make the distance measurement with the required accuracy (ref. 2). During these studies, standoff distance measurements were made using a metal reflecting plate to simulate a fully reflecting (critically dense) and lossless plasma. The use of metal reflecting surfaces to experimentally simulate plasma reflectance has been previously established (refs. 3-6). A theoretical analysis has been developed (ref. 7) that is capable of calculating the mutual coupling between two circular waveguide (CWG) apertures facing a flat metal surface with intervening homogenous dielectric layers. Thus, antenna apertures mounted in a ground plane with the apertures covered by a TPS and an ionized medium adjacent to the tile could be readily modeled. However, this model makes several idealizing assumptions that are not met in actual systems. The ground plane, dielectric layers, and the reflecting surfaces are assumed to have infinite planar dimensions, and the antenna apertures are assumed to have zero phase curvature or zero phase deviation. Since conical horn antennas were specified for the MRIS, laboratory experiments were devised to allow comparison of laboratory results using conical horns with the CWG model predictions. A scalar diffraction theory near-field model developed by R. W. Kreutel (*MRIS Antenna Design, A Status Report*, Electromagnetic Sciences, Inc., Norcross, Ga., Contract NAS1-19063, July 16, 1990) was available for predicting the signal power returned to the MRIS receiver from reflections in the antenna near-field. This model takes into account the range to the reflecting plate, the aperture diameter, and the aperture phase deviation of a given conical horn, but does not account for the effects of the parallel plate waveguide formed by the ground plane and reflecting plate. This near-field model approaches the Friis transmission equation or far-field equation near $2D^2/\lambda$. Complementary swept-frequency and CW reflection-coefficient measurements were

conducted for conical horn antennas mounted on a finite dimension ground plane in proximity to a finite dimension parallel reflecting plate. From the CW measurements, the effects of antenna aperture phase deviation and aperture efficiency were experimentally determined. The experimental swept-frequency measurements (not reported on here) provided complex reflection-coefficient data as a function of frequency and plate separation distances.

The CW experimental results are the subject of this memorandum and extend the plate separation distances of previous work (refs. 3, 5, and 6) to distances greater than 4.5λ . Also, the experimental data are essentially continuous as a function of plate separation distances rather than a series of discrete data points.

The purpose of this memorandum is to document the experimental CW results for three 2.2λ conical horns with aperture phase deviations of 6° , 23° , and 125° . Measurements of the magnitude of the reflection coefficient for each of the three 2.2λ antennas are presented as a function of plate separation distances. Each antenna was independently measured with and without a ground plane. Measurements were also made with and without a TPS tile over the aperture. The effects of possible plasma tilt on the magnitude of the reflection coefficient were experimentally determined by tilting the metal plate, which was normally parallel to the aperture plane.

3.0 Experimental System Configuration

For the laboratory evaluation of the MRIS concept that preceded the physical development of the flight instrument, it was not practical to test the actual flight component configurations. Therefore, representative components had to be chosen for simulated testing. In order to characterize the near-field to far-field behavior of conical horn antennas providing an order-of-magnitude frequency coverage for the MRIS on the AFE spacecraft, a representative frequency and a typical family of conical horns were selected for laboratory testing and evaluation. Availability of testing and measurement components resulted in a frequency choice of

24 GHz. Representative horn diameters for evaluation, based on typical D/λ values for the MRIS, resulted in a choice of 1.00 in. (2.54 cm) and 2.25 in. (5.72 cm). For the horn diameters thus selected for testing, a wide range of values for the aperture phase deviation was also chosen. The values chosen for the aperture phase deviation were 6° , 23° , and 125° . The aperture diameters and the phase deviations thus selected were based on normal engineering design considerations, such as physical similarity of test antennas to the actual flight antennas, frequency scaling, imposed physical constraints, and budgetary constraints. For brevity, only the laboratory measurement results of the 1.00 in. (2.54 cm) diameter apertures will be presented and discussed in this report. It is anticipated that a forthcoming report will address the measurement results for the larger diameter horns.

The CW reflectometer system shown in figure 1 was used to monitor and record the transmitted and received power. The other components used in the laboratory evaluation system included the antenna ground plane and reflecting plate, the TPS tiles, and the plate-positioning and vibration isolation systems. Details of all of the aforementioned pertinent components involved in the laboratory measurements are given in the following sections (3.1-3.5).

3.1 Reflectometer and Measurement Circuit

The 24 GHz reflectometer measurement circuit is shown in block diagram form in figure 2. All of the 24 GHz components were waveguide connected. A Gunn diode oscillator/isolator provided 100 milliwatts of power, with 30 decibels (dB) of isolation. A level-set attenuator (not shown in fig. 2) was used to adjust the power delivered to the antenna under test so that a power reflection coefficient of unity would produce full-scale deflection on the power monitors. Transmitted, or forward, power level was monitored through the -20 dB forward directional coupler, while the reflected or return power was monitored through the -6 dB reverse or return directional coupler. The precision attenuator that was permanently connected between the forward and return directional couplers was used to calibrate the measurement system (on a daily basis) in terms of the recorded power ratio in dB, between the transmitted and reflected power. This

power ratio, or power reflection coefficient, had a nominal measurement range of 0 to -35 dB.

Again, referring to figures 1 and 2, the forward and return power levels are sensed by frequency calibrated thermistor type power sensors and then converted into analog form for meter deflection and/or recording. For these measurements, the reflected power output was connected to a logarithmic voltage converter which provided an output voltage proportional to the logarithm of the power input. This voltage was recorded on an X-Y recorder, as a function of separation distance between the horn aperture plane and the reflecting plate.

3.2 Antennas

Since conical horn antennas were specified for the MRIS aperture, emphasis was given to laboratory testing and evaluation of representative flight reliable horns. As stated earlier, two diameters were selected for the apertures of the conical horns to be tested. For each aperture diameter, three aperture phase deviations were selected.

Table I identifies and gives an overall physical description for the 1.00 in. diameter antennas. Although all of the horn antennas had identical aperture diameters (D_a) of 1.00 in., the method of mounting the horns in the ground plane extended the cones and, due to different internal flare angles, resulted in slight differences in the effective (or actual) aperture diameters (D_e) at the ground plane. These diameters are given in Table 1 under the heading, Aperture Diameter, Effective.

3.3 Ground Plane and Reflecting Plate

Engineering design and necessity dictated that the antennas for the MRIS be physically mounted on the AFE vehicle's outer aluminum surface. The antenna apertures would be mounted flush with the metallic skin. Thus, the metallic skin of the AFE vehicle would provide a large ground plane for the MRIS antennas.

The highly reflective aspect of an overdense, electron-formed plasma layer to impinging RF energy can be simulated easily and inexpensively in the laboratory by the use of a metal reflecting surface (refs. 3-6). Therefore, for laboratory testing, a flat metal plate was chosen to provide the antenna ground plane, and a flat metal plate was also chosen to simulate the high RF reflection characteristics of the plasma.

The laboratory test fixture configuration is designed to simulate an MRIS conical horn antenna mounted on the AFE aerobrake with the aerobrake enveloped by a highly reflective plasma. This is accomplished by mounting the conical horn under test on a flat plate and measuring the magnitude of the RF reflection from an adjacent parallel flat plate. The measurements are made over a broad range of plate separation distances which span the range of distances in the plasma where total reflection is expected. To develop other laboratory measurement techniques (such as reflectometer measurements in an arc-jet facility) and to simulate AFE flight conditions (plasma generation) would not have been feasible considering the imposed budget constraints, availability of appropriate plasma-generating testing facilities, etc.

The decisions to use flat metal plates for system testing and the subsequent choice of plate dimensions were based on past practical experience and evidence in related experimental programs (refs. 3-6). Plates with large dimensions, in terms of electrical wavelength, could be more closely related to theoretical models where the plate dimensions were infinite.

The antenna ground plane and the reflecting plate were designed and fabricated with careful attention to surface finish and overall flatness. The surface finish for the plates was less than 32 micro-inches (0.00008 cm) and the overall surface flatness was less than 0.005 in. (0.0127 cm). Both plates were square with 18 in. (45.7 cm) sides. Overall dimensions in terms of electrical wavelengths were 36.6λ per side. Antenna-to-plate attachment was accomplished with the antenna mechanical boresite perpendicular to the ground plane.

3.4 Thermal Protection System (TPS) Tiles

A thermal protection system, similar to that used for the STS, was also employed to protect the integrity of the AFE aerobrake vehicle during the high enthalpy (high heating rate) portion of atmospheric reentry.

Like the STS system, the AFE TPS utilizes individual tiles to cover the exterior surfaces of the vehicle. To protect the waveguide-fed conical horn antennas on the AFE spacecraft from the extremes of temperature or from plasma contaminants, the antenna apertures had to be covered either with a lens or a window. In order to transmit RF information through a tile, a design decision had to be made either to cut an opening through the tile or to use the unaltered tile as a dielectric covering for the antennas. The latter choice was adopted. This necessitated a study of the RF characteristics of the tile material under simulated flight-type conditions. The room temperature tests described in this paper, using the TPS tile, were a part of the overall TPS study which included a high-temperature RF evaluation of the tile materials' transmission characteristics. The TPS study is documented by G. G. Heil in *High Temperature Electromagnetic Characterization of Thermal Protection System Tile Materials* (McDonnell Aircraft Co., St. Louis, Mo., Report No. MDC92B0034, Contract NAS1-18763, June 1992).

A representative TPS tile was used for the experiments described in this paper. The tile was a Lockheed LI-2200 silica-based material with a density of about 22 lbs/ft³ (0.35 g/cc). Dimensional characteristics for the tile are shown in figure 3. The overall size of the tile used was 6.0 in. (15.24 cm) by 8.0 in. (20.32 cm). As shown in the figure, the outer exposed surfaces of the tile were covered by a reaction cured glass (RCG) coating with a thickness of about 0.010 in. (0.025 cm). The most recent values for the electromagnetic properties of the tile materials at room temperature conditions (based on the TPS study results) are as follows: for the RCG coating, the relative permittivity was equal to 3.875 - j0.04; for the bulk tile material composing the core of the tile, the relative permittivity was equal to 1.335 - j0.003.

3.5 Plate Positioning System

A two-dimension positioning system, driven by stepper-motors, was used to position and control the distance and the relative angle between the antenna ground plane and the reflecting plate during measurements. The accuracy for the distance positioning was ± 0.0001 in./in. (± 2.5 microns/25 mm) and the accuracy for the tilt positioning was 3 arc min. As shown in figure 1, the entire measurement configuration including the microwave measurement system and the plate positioning system, was installed on an optical-type isolation table to eliminate the coupling of physical vibrations into the plate system. At a fixed or variable plate separation distance, small physical vibrations occurring between the plates could produce sizable oscillations in the amplitude of the measured signal. The isolation table was highly effective, and no amplitude variations in the measured data were due to plate vibrations.

Measurements were conducted with the antenna ground plane mounted in a fixed position on the optical table. The reflecting plate was movable in two dimensions, allowing either the separation distance between the plates or the relative angle of tilt between the plates to be varied. For range (distance) measurements, the plates were parallel. Angular (tilt) measurements were referenced to the parallel alignment of the plates.

The controller/stepper-motor could increase the plate separation in 0.0001 cm steps as a function of time, at rates of 0.0001 cm (1 step) per second to 10.0 cm (100,000 steps) per second. The rates selected here were 0.001 cm (10 steps) per second and 0.01 cm (100 steps) per second. The slower rate was used to provide a check to determine if the limited frequency response of the output recording device was affecting the data. The rates chosen for the plate-tilt measurements were 0.0167° (10 steps) per second and 0.167° (100 steps) per second.

4.0 Experimental Measurements and Discussion

Reflection-coefficient magnitude measurements for the $2.1 \lambda - 2.2 \lambda$ diameter conical horns are presented for the three horns. Table 1 provides individual horn identification as well as pertinent electrical and physical characteristics for each of the horns tested. The horn antennas are identified as horn B, D, and C and are listed in order of decreasing aperture phase deviations: 125° , 22.5° , and 6° . A physical comparison of the three horns can be seen in figure 4. Each of the experimental horns is mounted on a ground plane; except for minor differences in aperture diameters, the main physical differences between the horns are the taper lengths. The lengths noted in the figure are the taper lengths, that is, the axial distance from the aperture plane to the plane of the circular waveguide transition of the antenna feed. Also shown in figure 4, for comparison, is a pictorial representation of the theoretical CWG model antenna.

Comparison measurements of $|\Gamma|$, in dB, are presented in sections 4.1-4.8 and are shown as functions of distance to the reflecting plate (also stated as range distance or separation distance) and/or tilt angle of the reflecting plate. Measurements are presented for the horns listed in Table 1, as illustrated in figure 4. The data sets compare the various physical configurations used in the measurements, such as the comparison between conical horn apertures contained on a ground plane, and the same conical horn aperture without a ground plane. For each of the above conditions, measured data are presented both with and without the presence of an intermediate TPS tile.

4.1 Range Measurements

4.1.1 With Ground Plane, Without TPS Tile

Measurements of $|\Gamma|$ versus plate separation distance for each conical horn (B, D, and C) mounted on a ground plane, without an intermediate TPS tile, are shown in figures 5, 6, and 7. For these measurements, the reflecting plate was moved from an aperture shorted condition (0 cm) to a separation distance of 20 cm. In each figure, the resultant $|\Gamma|$ can be seen

to vary with distance with a periodicity of $\lambda/2$ between maximums. An overall comparison of $|\Gamma|$ versus range in figures 5, 6, and 7 shows that the data from the different horns is very similar. With the exception of the close-in range ($0 < d < \mathbf{FF}$) for horn B, as shown in figure 5, the peak magnitudes have nearly identical $|\Gamma|$ values as a function of range distance. From the figures it is obvious that the main difference between the three cases is the degree of the rapid magnitude versus distance variations in $|\Gamma|$ when $|\Gamma|$ is small. These variations are attributed to parallel-plate waveguide propagation and edge effects and are the subject of further study. For purposes of the MRIS measurements it was desirable to obtain a return signal from the reflecting plate with a magnitude as large as possible. While parallel-plate propagation is related to plate separation, the small variations in $|\Gamma|$ due to this effect are detrimental to the measurement of plate separation by the method used in the MRIS experiment. Referring to figures 5-7, for range distances greater than the far-field boundary (\mathbf{FF}) where ($\mathbf{FF} < d < 20$ cm), it appears that the antenna with the larger aperture phase deviation has less severe $|\Gamma|$ variation in the null region.

Expanded time-base measurements made at selected ranges within figures 5-7 are presented in figures 8-10. The calculated far-field boundary ($2D^2/\lambda$) is given in part (b) of the figures for each of the apertures. Thus, in figure 8, for horn B the \mathbf{FF} is 12 cm. In parts (a) and (c) of figure 8, the selected ranges are near $\mathbf{FF}/2$ (6.0 cm) and $3\mathbf{FF}/2$ (18 cm), respectively. The same reasoning was used to establish the range values given in figures 9 and 10. The reason for choosing range blocks of 2 cm about the selected ranges was to show the effect of several continuous $\lambda/2$ distance increments.

As in the 0-20 cm ranges shown in figures 5-7, the cyclic behavior can be readily seen in figures 8-10, where the maximums occur for every $\lambda/2$ of plate separation. There are several distinguishing features between data contained in the three graphs. First, notice the increasing sharpness of the maximum peaks as distance is increased from (a) to (b) to (c). This is consistent with theoretical results (ref. 3, p. 20). Notice the increasing amplitude variation within the regions between the $\lambda/2$ peaks, as the plate distance is increased from (a) to (b) to (c). This may be due to the fact that more propagating modes exist as the spacing between the plates is

increased. Again, comparing (a) to (b) to (c), the number (or frequency) of the smaller variations between $\lambda/2$ peaks decreases as the plate distance is increased. A physical interpretation of this behavior is that the electrical length of the open-ended waveguide formed by the parallel plates decreases as plate spacing is increased and is most sensitive to plate spacing immediately after the onset of a new propagating mode, because of the relationship of group velocity in the guide to the plate spacing (ref. 8). This is consistent with the observed behavior.

Similar to the overall comparison between figures 5-7 described above, an overall comparison between figures 8-10 reveals many similarities in $|\Gamma|$ as a function of the **FF** range. The major difference between the figures is the relative sharpness (relative slope with increasing distance) of the $|\Gamma|$ data immediately before it peaks. The $|\Gamma|$ data for horn B, in figure 8, appears much sharper than that for either of the other horns. For horns D and C, in figures 9 and 10, respectively, the $|\Gamma|$ data as a function of **FF** range appear almost identical. A fully theoretical explanation for this behavior was not developed.

4.1.2 With Ground Plane, With TPS Tile

Figures 11-16 are measurements of $|\Gamma|$ with a TPS tile spaced 0.160 in. (0.406 cm) from the ground plane, as is the case of the AFE aerobrake where each tile is attached to the vehicle's surface by a 0.160 in. layer of strain relief material. The strain relief layer was omitted here because it was excluded in the immediate neighborhood of the MRIS antenna apertures in the flight configuration on the AFE vehicle. (In the flight configuration, the presence of the lossy strain relief layer in the vicinity of the apertures could be expected to somewhat mitigate the effects of the metal groundplane, thus this experimental configuration can be considered a worst case for ground plane effects.) The reflecting plate separation distance as shown in figures 11-16 are always given with respect to the antenna aperture plane although the closest possible plate-to-plate spacing is 1.255 in. (3.1877 cm).

The character of the $|\Gamma|$ data with the TPS tile present, shown in figures 11-16, are quite different from those without the tile (shown in figs.

5-10). The tile significantly reduces the corresponding peak amplitudes of $|\Gamma|$, particularly with $\phi = 125^\circ$. In addition, the cyclic $\lambda/2$ behavior is not as well defined as in figures 5-10. Also, the depths of the nulls are much lower with the tile, and although the null depth excursions appear to be periodic, they vary more erratically with small changes in distance.

Large values for $|\Gamma|$ mean, by definition, a poorer impedance match between the radiating antenna and its surrounding medium. Conversely, small values for $|\Gamma|$ mean that the impedance match improves between the radiating antenna and its surrounding medium, thus, allowing more energy to escape the antenna aperture and the ground-plane to reflecting medium system (TPS tile and reflecting plate). With the above discussion in mind, it appears that the addition of the TPS tile between the ground plane and reflecting plate increases radiation. It is also obvious, by comparing figures 8-10 with those of figures 14-16, that the use of TPS tile spreads the peak energy returns more uniformly across the 2-cm range block. This is evidence of the effects of multiple internal and external reflections caused primarily by the RCG coating on the tile. The internal reflections (those occurring between the tile surfaces and the ground plane) are independent of plate spacing and tend to reduce the $\lambda/2$ variations in $|\Gamma|$. The external tile reflections vary as the distance between the RCG coating and the reflecting plate and thus reduce the $\lambda/2$ variations due to the stronger plate-to-plate reflections.

4.1.3 Without Ground Plane, Without TPS Tile

Figures 17-19 are measurements of $|\Gamma|$ as functions of d , for conical horns B, D, and C, respectively, with the antenna ground plane removed and the area behind the horn covered with an RF absorber to eliminate extraneous reflections. That is, the antenna under test is a conical horn without a ground plane.

As can be seen in figures 17-19, $\lambda/2$ periodicity is apparent in the data over the entire 20 cm plate separation distance; but now, the periodic wave form has a sinusoidal shape with a peak-to-peak minimum variation of about 3 dB that is independent of d . Obviously, removing the ground plane from

the antenna system eliminates parallel plate waveguide effects. This can be seen by comparing figures 17-19 with figures 5-7. The nearly constant dB-ripple in $|\Gamma|$ versus d for figures 17-19 was postulated (by Kreutel based on his scalar diffraction theory model) as higher-order mode effects in the throat of the horns in the absence of a ground plane. When the antenna aperture is on a ground plane, the dominant secondary (second bounce) reflection is greatly increased. Figures 20 and 21 are expansions of selected regions within figures 17 and 19, respectively, where distances from 4 to 6 cm and 10 to 12 cm are shown with the expanded time base. (Since the curves are monotonic, only one expanded time-base block is shown for each of horns B and C.)

A comparison of figures 17-19 shows that the larger phase taper ($\phi = 125^\circ$) produces $|\Gamma|$ about 3 dB less than the smaller-taper cases, whereas $|\Gamma|$ versus d for both figures 18 and 19 are almost identical.

4.1.4 Without Ground Plane, With TPS Tile

For figures 22, 23, and 24, the TPS tile is placed between the conical horn aperture and the reflecting plate. As before, there is a 0.160 in. (0.406 cm) offset distance between the aperture plane and the tile surface. The figures show the resultant $|\Gamma|$ as a function of distance to the reflecting plate. The shape of the $|\Gamma|$ peaks are very similar to those when no tile is used as seen in figures 17-19. Comparing figures 22-24 with figures 17-19, particularly at the larger distance ranges, it is obvious that when the tile is used the minimum $|\Gamma|$ is decreased (increasing the maximum radiation loss) and the maximum $|\Gamma|$ is increased.

Figure 25 has an expanded distance scale similar to figure 21. A direct comparison of figures 25 and 21 clearly shows the effects of the TPS tile on the reflection coefficient when no ground plane is used.

4.2 Tilt Measurements

4.2.1 With Ground Plane, Without TPS Tile

For non-tilt measurements, the radiating antenna was always aligned with normal incidence to the reflecting plate. This condition simulated reflection characteristics from a reflective medium, such as an ionized plasma, that would be normal to the boresite of a forward sensing antenna located in the stagnation region. It was expected, however, that due to spacecraft small angle-of-attack motions, the ionized plasma could have small angles of tilt referenced to the forward looking antennas. For the reason stated above, laboratory reflection measurements were conducted with the reflecting plate tilted with respect to the antenna. All tilt-measurements were performed by rotating the reflecting plate about an axis which was normal to and intersecting the antenna boresite axis, while the antenna was in a fixed position and the distance range was held constant. The actual spacing (d) was deviated slightly about the nominal values given in the figures so that $|\Gamma|$ (at zero tilt) was maximized. (This corresponds to the peak values as shown in figures 5-7). For reflecting plate tilt angle measurements on either side of 0° (the peak value for $|\Gamma|$), the term used in this report to describe the included tilt angle values of $|\Gamma|$ that are 3 dB less than peak, is tilt width.

Figures 26-28 show $|\Gamma|$ data for four plate-separation distances for antennas B, D, and C as the reflecting plate is rotated about the tilt axis. These figures are for the horns mounted in a ground plane with their effective diameters (D_e) indicated. The three figures show that peak $|\Gamma|$ near normal incidence is very sharp and narrow, with the -3 dB maximum tilt widths extending from $\pm 1.0^\circ$ to $\pm 2.0^\circ$ at plate distances of 5 cm. Again, comparing the three figures, the -3 dB tilt width increases slightly with decreasing aperture phase deviation. For each horn the tilt width becomes narrower as the range distance is increased, as is evident in the figures. The distances and the values for $|\Gamma|$, as shown, are the same values of $|\Gamma|$ occurring in figures 5-7, respectively, for reflecting plate distances of 5, 10, 15, and 20 cm.

4.2.2 With Ground Plane, With TPS Tile

Figures 29-31 are physically the same configurations as shown in figures 26-28, except the TPS tile has been placed in a fixed position between the ground plane and the reflecting plate, with the tile offset 0.406 cm from the antenna aperture plane. The $|\Gamma|$ for tilt measurements in the figures with the TPS tile has a much different character than those shown without the tile. In figures 29-31, although there are individual variations of 10 dB or less within a $\pm 7^\circ$ tilt angle change for each of the range distances, essentially all of the $|\Gamma|$ data are contained within the -2.5 dB to -23 dB level. In comparison, for tilt angle changes of $\pm 5^\circ$ to $\pm 7^\circ$, as seen in figures 26-28 with no TPS tile, $|\Gamma|$ can decrease in value from -10 dB to -25 dB as the separation distance is increased only slightly. (Particularly, note range distances of 15 and 20 cm in these figures). This provides confirmation that the use of the TPS tile spreads the effective return from the reflecting plate while it reduces the sharpness of the peak returns at $\lambda/2$ intervals. Also, a comparison of figures 29-31 shows that the peaks of the $|\Gamma|$ response around 0.0° tilt angle become more visible with decreasing aperture phase curvature. Clearly, the TPS tile has a major effect on the characteristics of the radiating system.

4.2.3 Without Ground Plane, Without TPS Tile

The magnitude of the reflection coefficient for conical horns B, D, and C without the ground plane and as a function of reflecting plate tilt are shown in figures 32, 33, and 34, respectively. The same distances, as shown in sections 4.5 and 4.6 above, are shown. $|\Gamma|$ is maximum at normal plate incidence and decreases smoothly and gradually as tilt is increased. For conical horn B with an aperture phase deviation of 125° , the -3 dB tilt width is $\pm 8.5^\circ$ at a separation distance of 10 cm and $\pm 8^\circ$ at a distance of 20 cm. Conventional antenna pattern measurements provided by the manufacturer of horn B show **E**- and **H**-plane -3 dB beamwidths of 27.8° and 30.7° , respectively. Horn-to-horn beamwidth measurements, with no ground plane used, confirmed the manufacturer's data. In comparison, for conical horn C with an aperture phase deviation of 6° , the -3 dB tilt width is $\pm 10^\circ$ at a separation distance of 10 cm and $\pm 7.5^\circ$ at a distance of 20 cm.

4.2.4 Without Ground Plane, With TPS Tile

Figures 35 and 36 (for conical horns D and C) with aperture phase deviations of 22.5° and 6° , exhibit an almost flat response for $|\Gamma|$ at plate separation distances of 10, 15, and 20 cm. Data for conical horn B ($\phi = 125^\circ$) was not available for this particular data set. Comparing figures 33 and 34 (where there was no ground plane or TPS), with figures 35 and 36, shows again the TPS spreading effect on the reflection coefficient as a function of reflecting plate tilt.

5.0 Theoretical Models and Comparison with Experimental Results

Computer codes were available which can predict the RF reflection levels or antenna mutual coupling effects for a CWG antenna mounted on a ground plane and illuminating a parallel reflecting surface (ref. 7). These theoretical models make certain assumptions that cannot be physically modeled in a laboratory experimental setup. The theoretical model assumes that the antenna has zero phase deviation across the aperture. In order for an actual conical horn antenna to have zero phase deviation across the aperture, the antenna would either have to be infinitely long or have a phase correction lens placed in the aperture. The model also assumes that within the antenna system, all surfaces, including the ground plane and the reflecting plate, have infinite dimensions.

Figure 37 shows a theoretical prediction, using the CWG model, of the magnitude of the reflection coefficient as a function of separation distance for a 2.7-cm diameter circular waveguide antenna. The notations within the figure describe the antenna system's characteristics.

The characteristics of conical horn C, with an aperture phase deviation of 6° , offer the closest comparison with the CWG model. A comparison of the reflection coefficient magnitudes of figure 37 with those shown in figure 7 reveal good general agreement. The major difference between the two sets of data is the character of the reflections occurring in the null regions

between the $\lambda/2$ peaks. In these null regions, the experimental data contain rapidly varying $|\Gamma|$ with small distance changes while the CWG model results are smooth and exhibit no rapidly varying fluctuations. This phenomenon within the nulls is believed to be the result of the fact that the finite parallel plates act as an open-circuited mismatched waveguide that produces reflections with phase varying as the plate spacing is increased. Therefore, the different results for the CWG model in the null areas appear to be due mainly to the assumption of infinite transverse planes that cannot be duplicated in the experiments.

Figure 38 compares maximum and minimum values of $|\Gamma|$ as a function of discrete \mathbf{D}^2/λ ranges for the three 2.2λ conical horns. The respective aperture phase deviations for the horns are also shown in the figure. For the null areas of the experimental data, the average value of $|\Gamma|$ is indicated. The experimental results of both horn C and horn D agree well with the CWG model.

The scalar diffraction theory near-field model, developed by Kreutel, was available to predict the signal power returned to the MRIS receiver from reflections in the antenna near-field. This model takes into account the range to the reflecting surface (reflecting plate), the aperture diameter, and the aperture phase deviation of a given conical horn. The model does not account for the effects of the parallel plate waveguide formed by the ground plane and reflecting plate. This near-field model approaches the Friis transmission equation or far-field equation near $2\mathbf{D}^2/\lambda$.

Figure 39 shows a comparison between the scalar diffraction theory predictions and the experimental measurements for a conical horn antenna ($\mathbf{D} = 2.74 \text{ cm}$; $\phi = 125^\circ$). The experimental measurement results of $|\Gamma|$ versus \mathbf{d} are the same as shown in figure 5. For the experimental measurements, the conical horn was mounted on the ground plane, as shown in figure 4(a). The scalar diffraction theory model, however, does not account for ground plane effects. As is evident in figure 39, the diffraction model predictions (shown by the heavy line) have values of $|\Gamma|$ that are +3 dB to +4 dB greater than the average null values of the experimental measurements.

Figure 40 is a comparison of the scalar diffraction theory predictions and the experimental measurements for the conical horn shown in figure 39 ($D = 2.74$ cm; $\phi = 125^\circ$), but without a ground plane. The experimental measurement results of $|\Gamma|$ versus d , as shown in figure 40, are the same as shown in figure 17. Figure 40 shows the good agreement, for values of $|\Gamma|$, between the diffraction model predictions (shown by the heavy line) and the average value of the experimental measurements.

6.0 Conclusions

Measurements have been made of the magnitude of the reflection coefficient occurring in an experimental model antenna system. The laboratory system was composed of 2.2λ diameter conical horns having a range of aperture phase deviations mounted on a ground plane and illuminating a parallel flat metal plate through an intervening TPS tile. The measurements were performed through a range of plate separation distances and plate tilt angles.

The major emphasis of the measurements described in this report was to verify theoretical analyses in support of development of the MRIS instrument. The general experimental goals are described in the following paragraphs.

The measurement results were used to substantiate near-field and far-field transmission efficiency levels for a MRIS-type propagation path. The various conical horns used in this experiment were chosen to evaluate the influence of aperture phase deviation on the transmission efficiency. Measurement results were also used to assess the impact of the AFE stagnation-region TPS tile on the transmission efficiency. The various transmission efficiency evaluations using the experimental model have been successful and will be discussed in a future publication.

Measurement results indicate, for the same physical conditions, that there are minor differences in $|\Gamma|$ for the conical horns with the smaller

aperture phase deviations. The horn with an aperture phase deviation of 125° consistently exhibited lower $|\Gamma|$ than similar measurements for the other horns.

Based on these experimental results, the MRIS design requirement to radiate through the TPS tile structure appears to be acceptable. When the TPS tile is part of the antenna system, the severe $|\Gamma|$ fluctuations at $\lambda/2$ range intervals are reduced and the effective antenna beam is broadened. These effects are primarily due to the presence of the RCG coating which gives rise to a combination of internal and external reflections. Although the effects identified do not indicate a problem, the overall effect of the TPS on the ability of the MRIS system to measure distance can not be determined based on the data presented here, and the issue continues to be studied.

The results of this study were used to ascertain the effects of the TPS tile on MRIS design specifications such as: signal-to-noise ratio, signal-to-interference ratio, and receiver dynamic range. Insight and confidence was provided by these continuous wave ranging measurement results. These experimental results were supportive of a parallel laboratory measurement effort to measure the time domain properties of a MRIS-type propagation path. Finally, the laboratory measurements indicate the general validity of the CWG theoretical model for predicting the general behavior of the parallel plate geometry. CWG predicted the $\lambda/2$ peaks and the depth of the troughs. CWG did not predict (nor was it expected to predict) the ripple effects occurring in the troughs. The laboratory measurements also indicate the general validity of the scalar diffraction theory model in the absence of parallel plate geometry. The scalar diffraction theory model predicted the general behavior of the mean $|\Gamma|$ versus d . The scalar diffraction theory model did not predict the $\lambda/2$ peaks or the ripple effect on $|\Gamma|$ as a function of d . The experimental measurements tied the CWG theoretical model results and the scalar diffraction theory model results together. The reasonable agreement between theoretical and experimental models provided increased confidence in the MRIS design.

7.0 References

1. Grantham, W. L.: Flight Results of a 25,000-Foot-Per-Second Reentry Experiment Using Microwave Reflectometers to Measure Plasma Electron Density and Standoff Distance. NASA TN D-6062, December 1970.
2. Neece, R. T.; Cross, A. E.; and Schrader, J. H.: The MRIS Feasibility Study. NASA TM-107763, April 1993.
3. Jones, J. E.; and Swift, C. T.: The Aperture Admittance of a Ground-Plane-Mounted Waveguide Illuminating a Perfectly Conducting Sheet. NASA TM D-4336, March 1968.
4. Jones, J. E.; Tsai, L. L.; Rudduck, R. C.; Swift, C. T.; and Burnside, W. D.: The Admittance of a Parallel-Plate Waveguide Aperture Illuminating a Metal Sheet. IEEE Transactions on Antennas and Propagation, Vol. AP-16, No. 5, September 1968.
5. Hearn, C. P.; Bailey, M. C.; Czerner, M. J.; Dudley, K. L.; and Vedeler, E.: An Assessment of the Potential of Continuous-Wave Ranging for Measuring the Distance to a Highly Reflective Infinite Sheet. NASA TM-101680, April 1990.
6. Bailey, M. C.; Beck, F. B.; Croswell, W. F.; Jones, J. E.; and Swift, C. T.: Waveguide Antennas Illuminating a Metal Sheet. IEEE Transactions on Antennas and Propagation, Vol. AP-18, No. 3, May 1970.
7. Bailey, M. C.: CWG - A FORTRAN Program for Mutual Coupling in a Planar Array of Circular Waveguide-Fed Apertures. NASA TM-101614, June 1989.
8. Jordan, E. C. and Balmain, K. G.: Electromagnetic Waves and Radiating Systems, 2nd Edition. Prentice-Hall, 1968.

Table I. $2.2\text{-}\lambda$ Diameter conical-horn antenna characteristics, electrical and physical

Antenna Identification Series	Aperture Phase-Deviation (Actual)		Effective Aperture Diameter, D_e , (Mounted on groundplane)			Aperture Diameter, D_a (No groundplane)			Far Field Range, cm ($2D^2/\lambda$)	
	λ	degrees	λ	cm	inches	λ	cm	inches	D_e	D_a
B	0.35	125.0	2.2	2.74	1.08	2.03	2.54	1.00	12.0	10.3
D	0.06	22.5	2.1	2.62	1.03	2.03	2.54	1.00	11.0	10.3
C	0.02	6.0	2.1	2.57	1.01	2.03	2.54	1.00	10.5	10.3

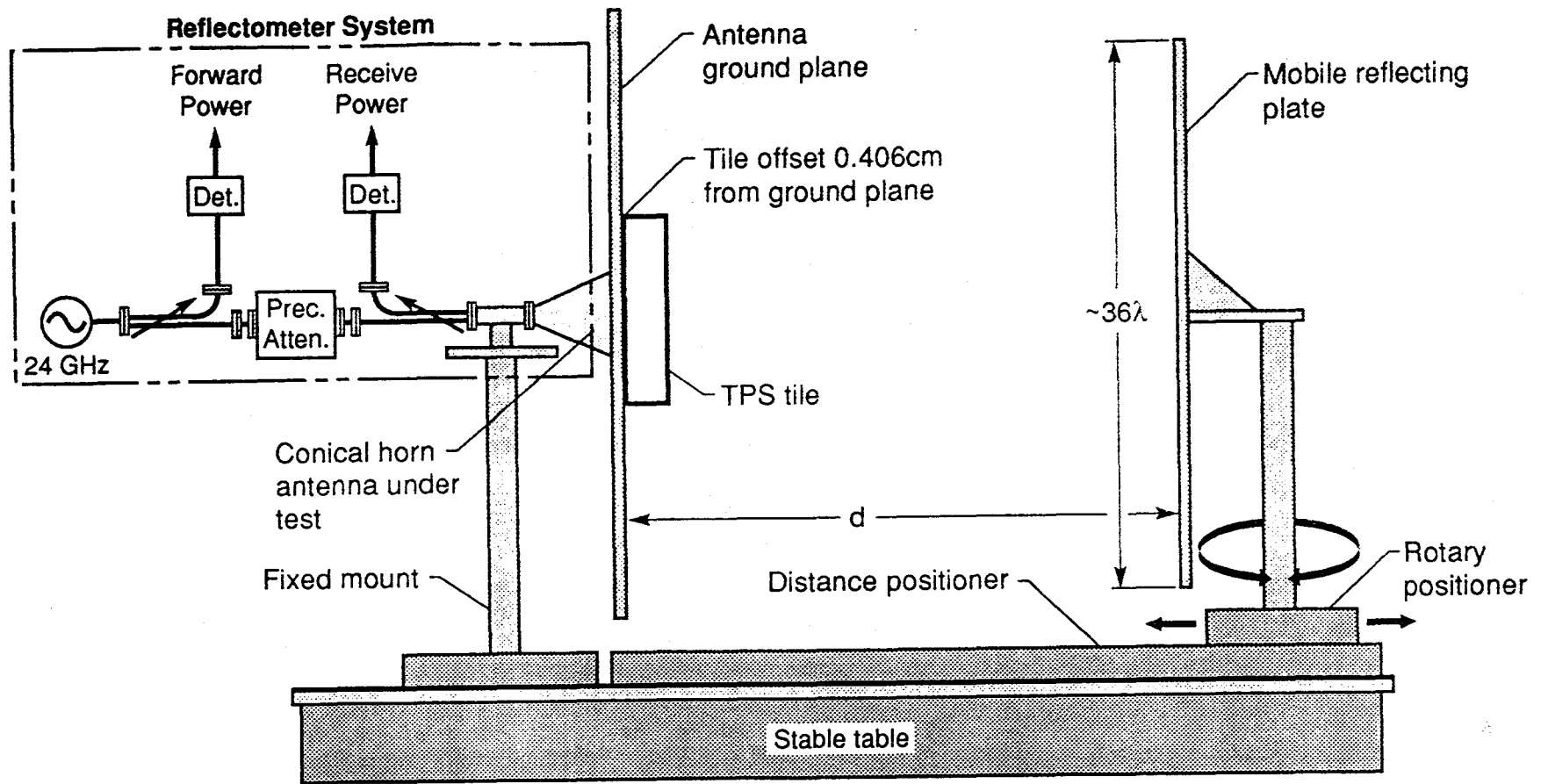


Figure 1. Simplified baseline experimental-system configuration.

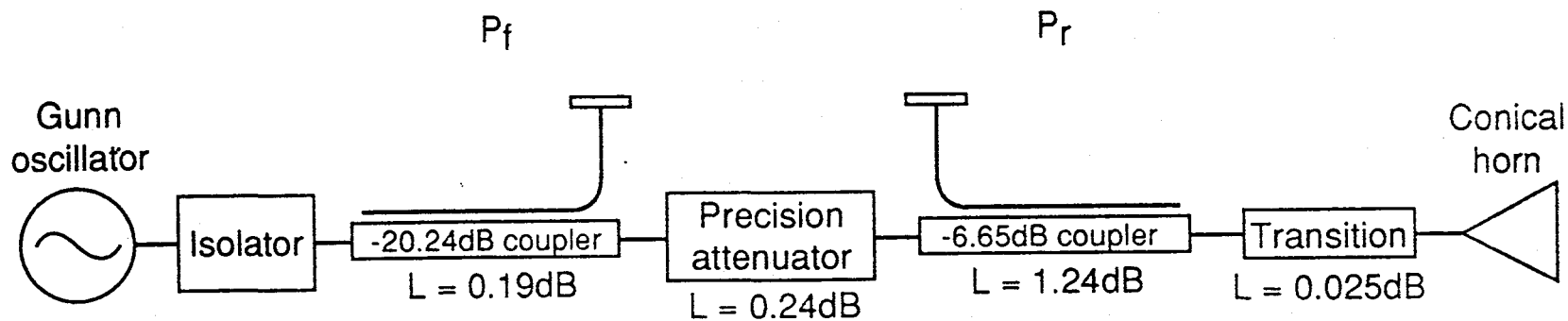
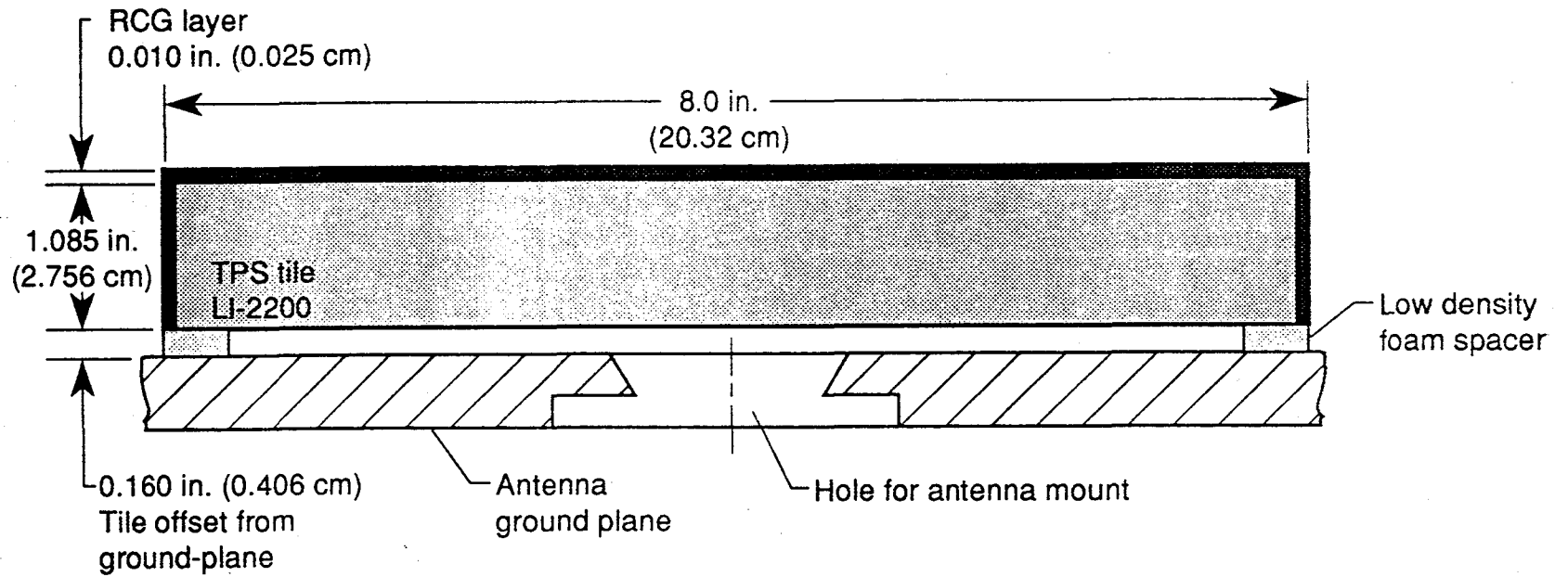
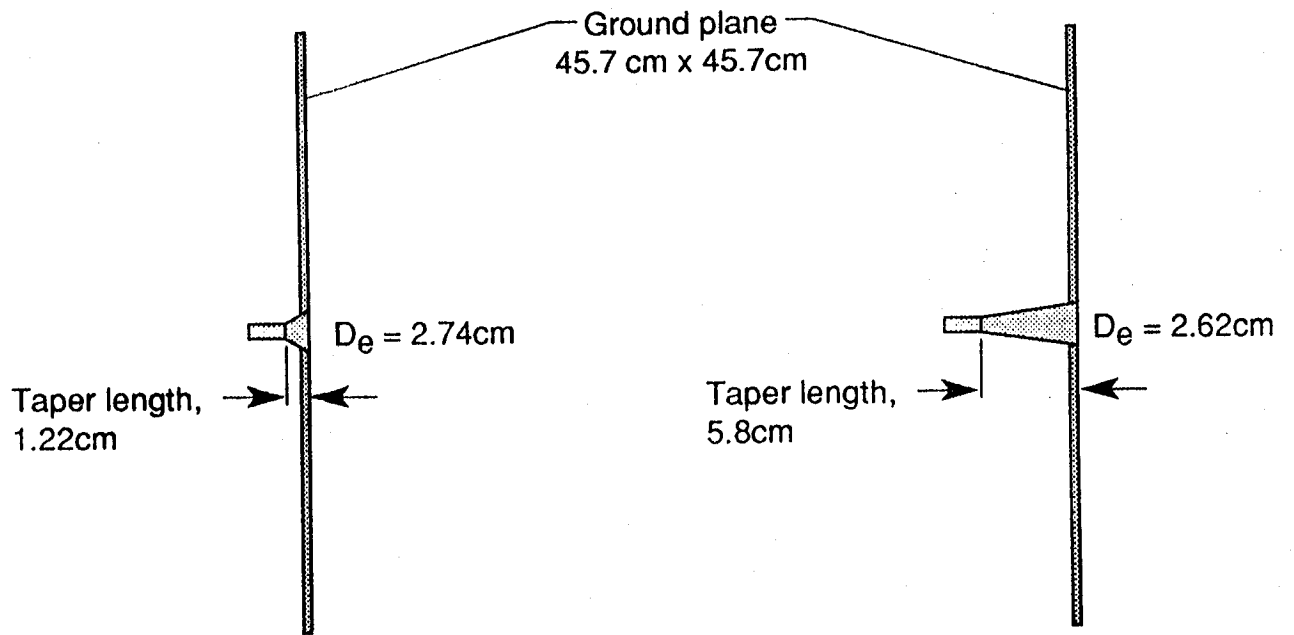


Figure 2. 24GHz reflectometer measurement circuit.



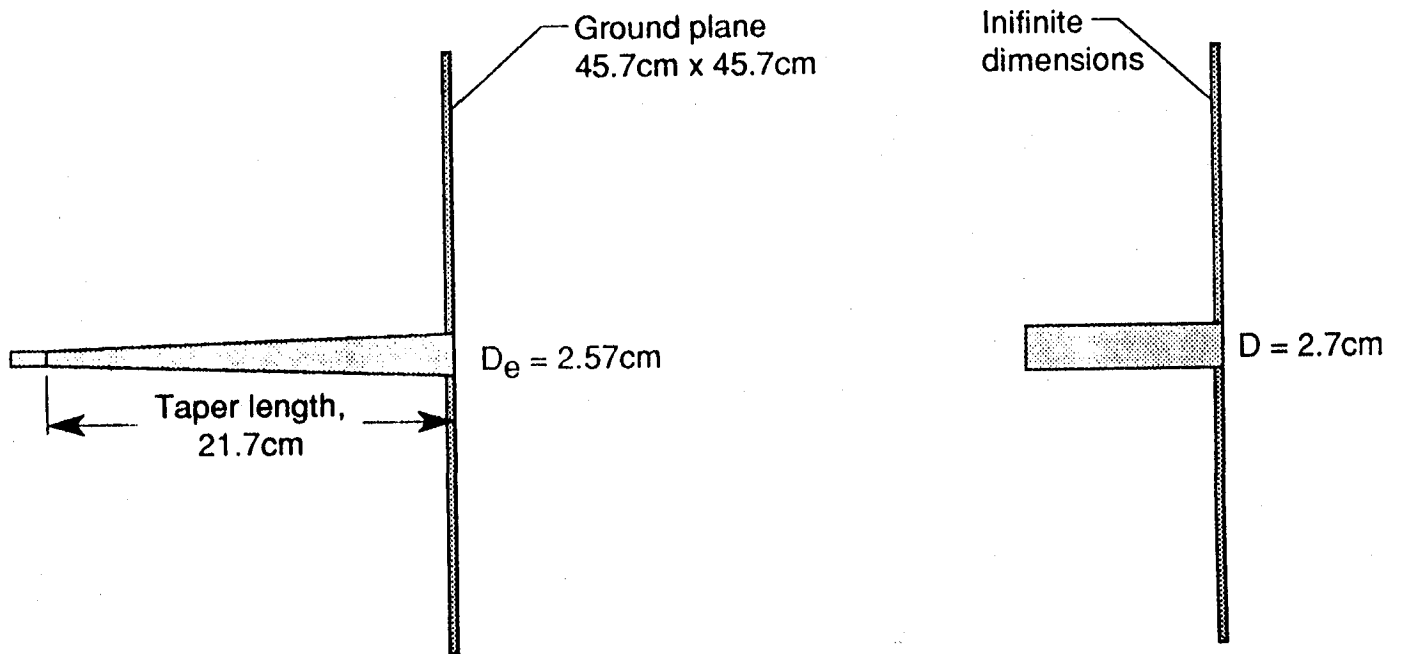
Not to scale

Figure 3. Dimensional characteristics of TPS test tile.



(a) Conical horn B; $\phi = 125^\circ$

(b) Conical horn D; $\phi = 22.5^\circ$



(c) Conical horn C; $\phi = 6^\circ$

(d) CWG antenna; $\phi = 0^\circ$

Figure 4. Relative physical-comparison between experimental and theoretical antenna systems.

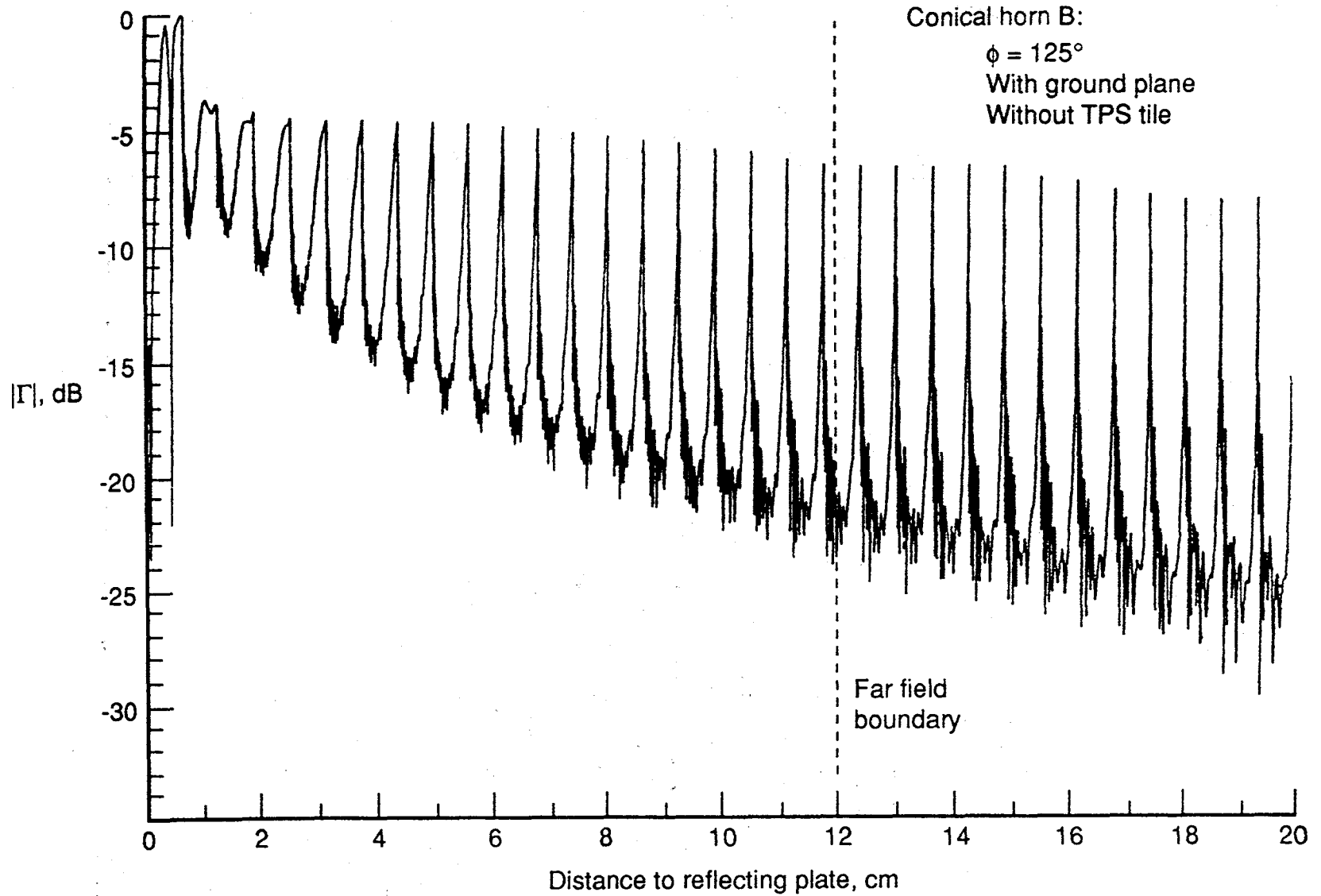


Figure 5. $|\Gamma|$ as a function of plate-separation distance for a 2.74 cm diameter horn with 125° aperture phase taper.

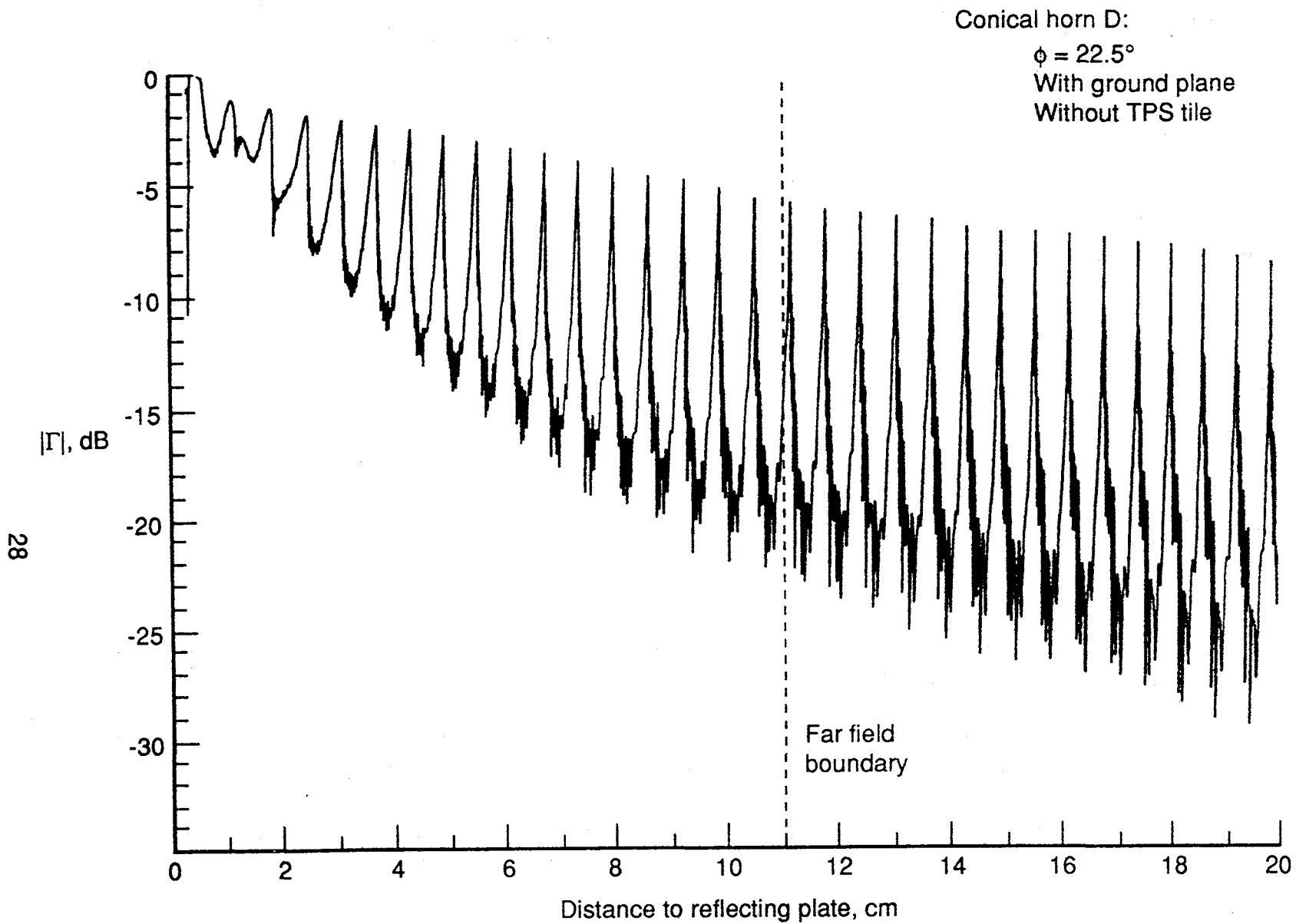


Figure 6. $|\Gamma|$ as a function of plate-separation distance for a 2.62cm diameter horn with 22.5° aperture phase taper.

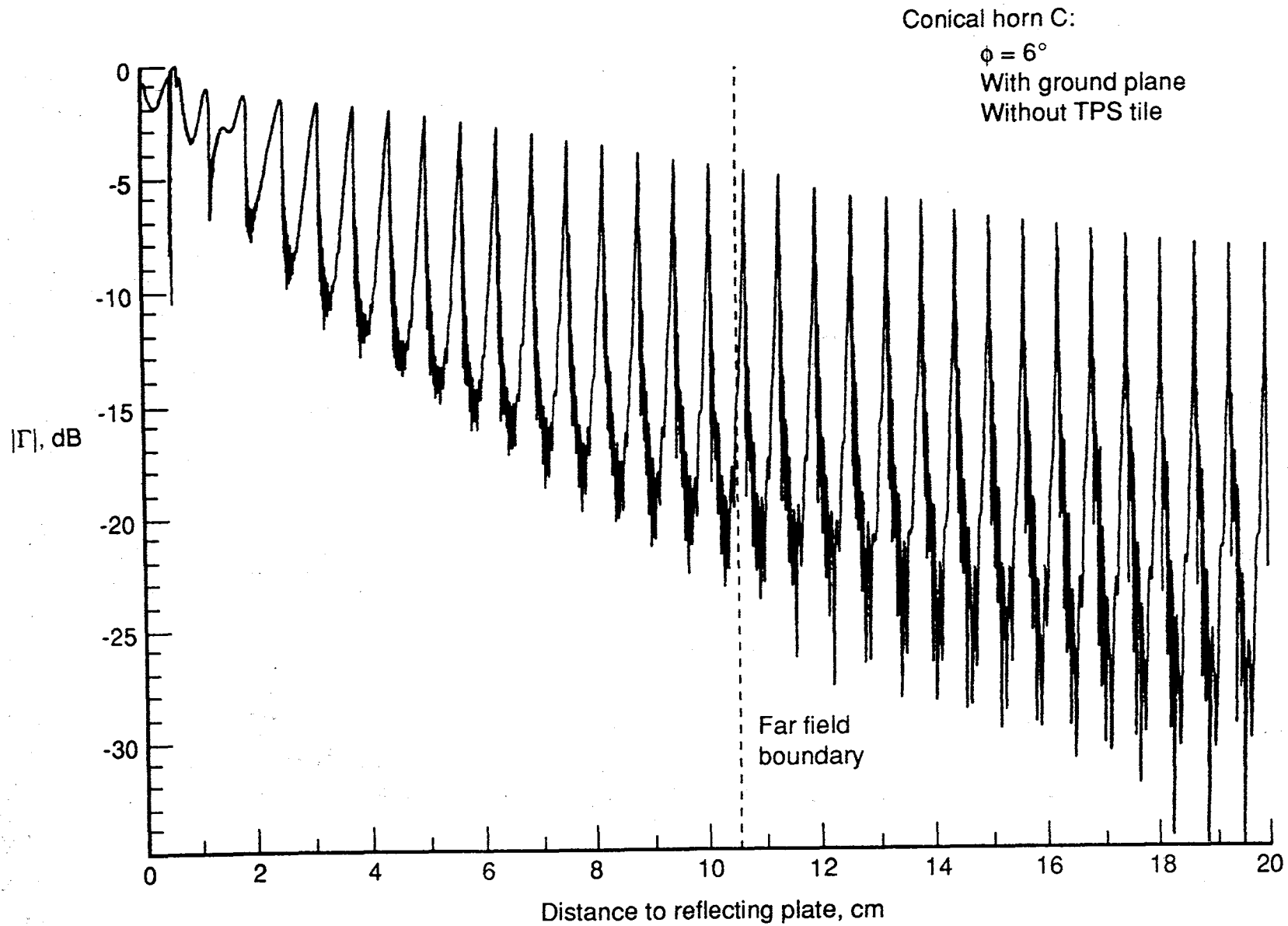


Figure 7. $|\Gamma|$ as a function of plate-separation distance for a 2.57cm diameter horn with 6° aperture phase taper.

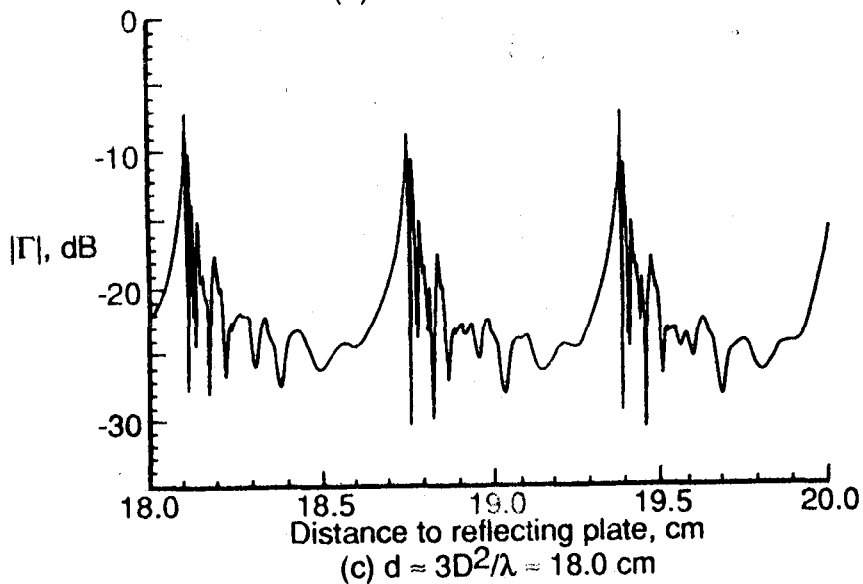
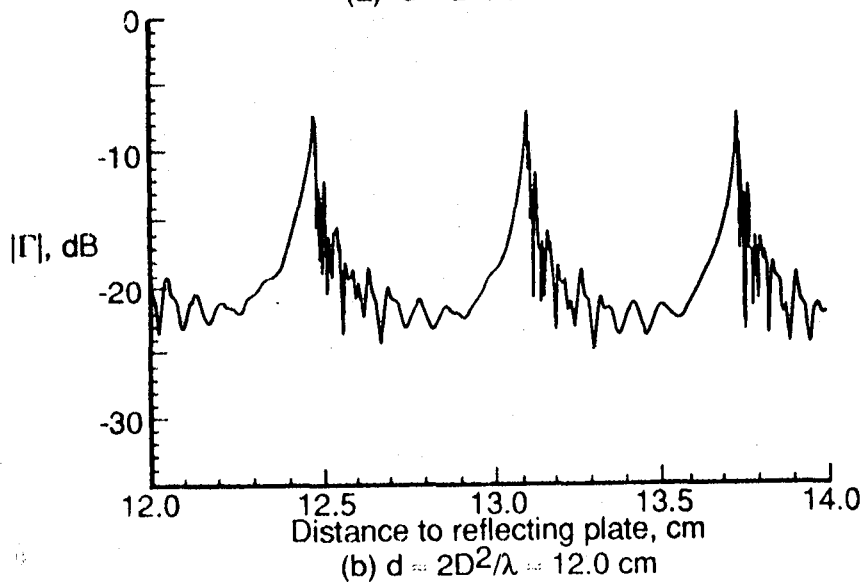
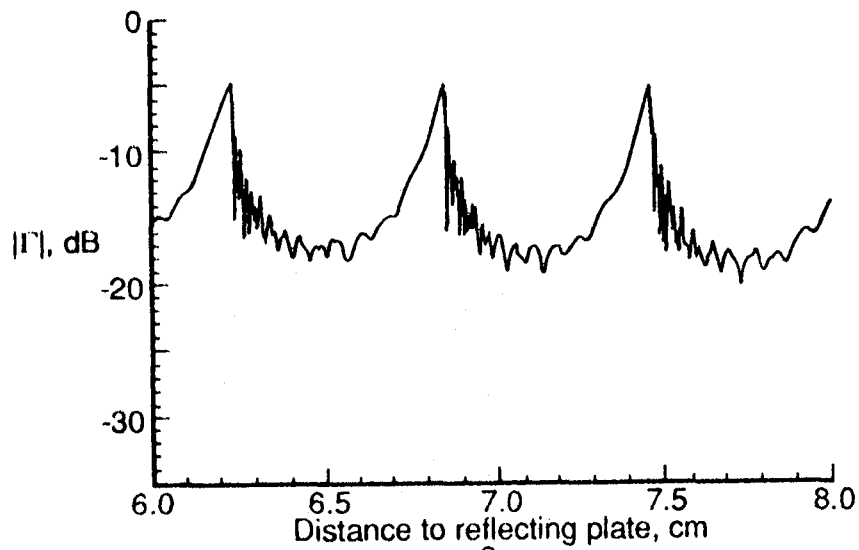


Figure 8. $|\Gamma|$ as a function of range for three plate-separation distances for a 2.74 cm diameter horn; with ground plane, without TPS tile, conical horn B, $\phi = 125^\circ$.

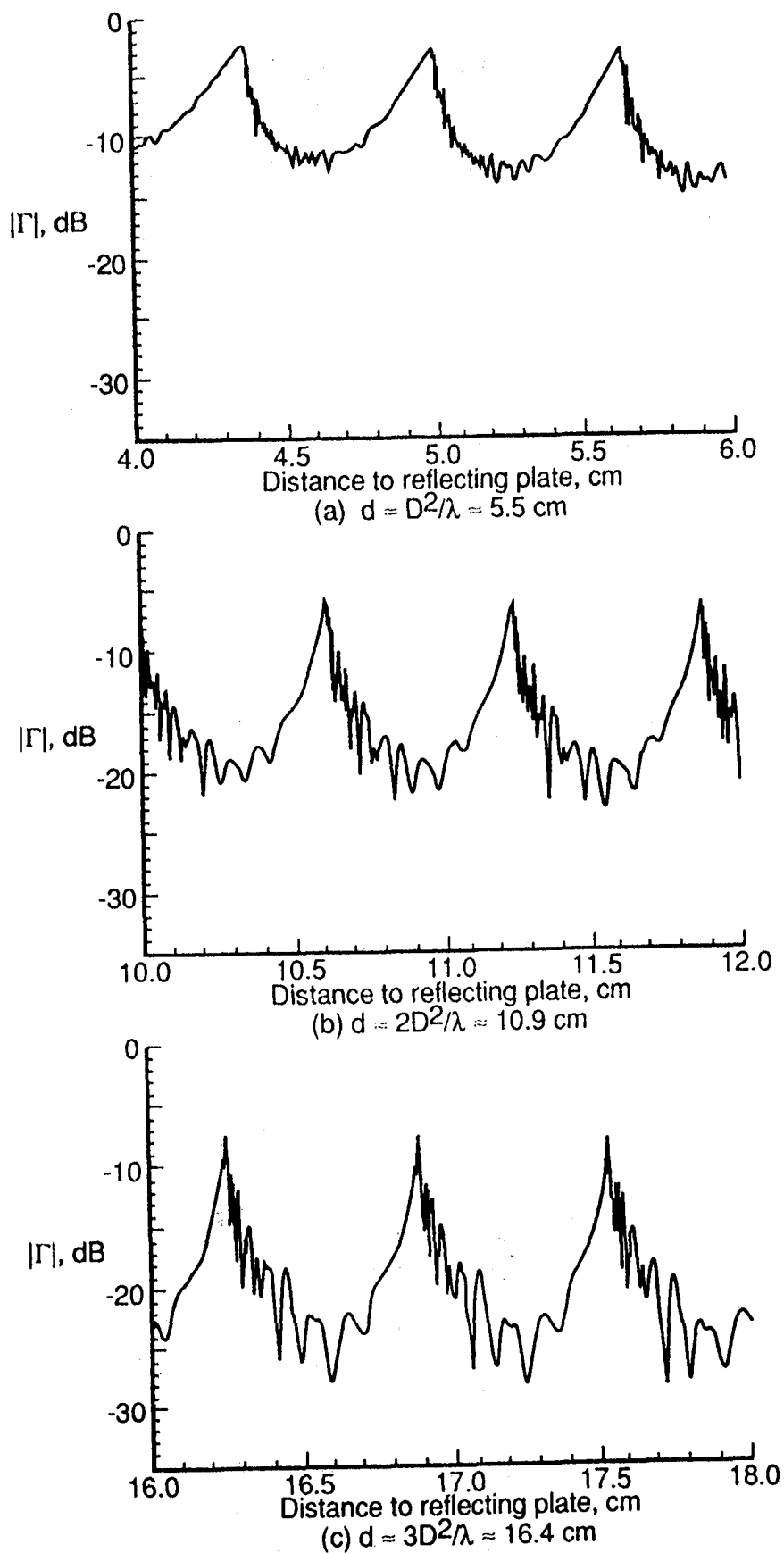


Figure 9. $|\Gamma|$ as a function of range for three plate-separation distances for a 2.62 cm diameter horn; with ground plane, without TPS tile, conical horn D , $\phi = 22.5^\circ$.

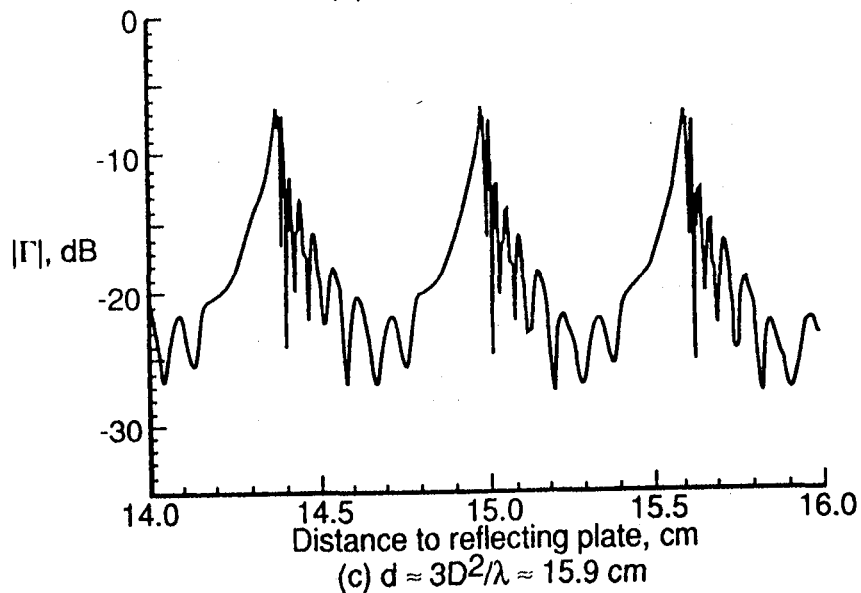
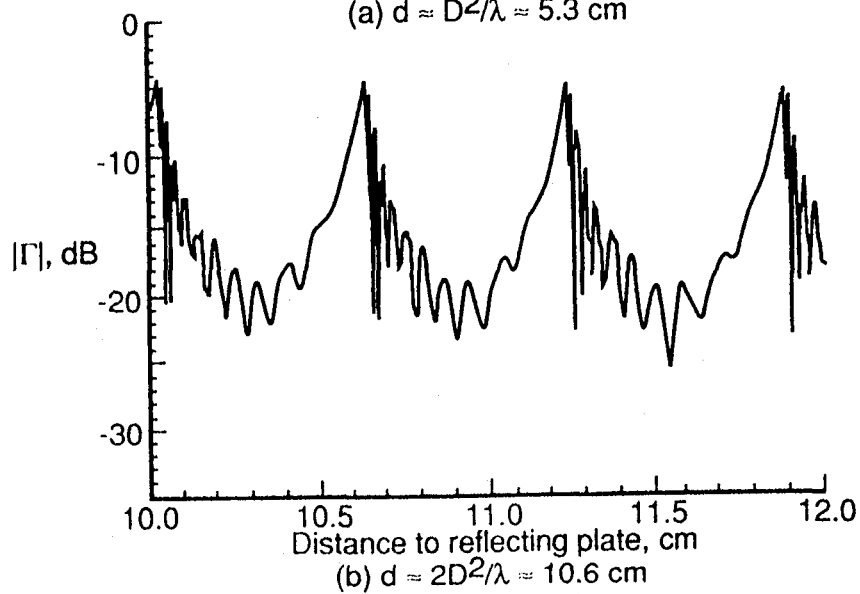
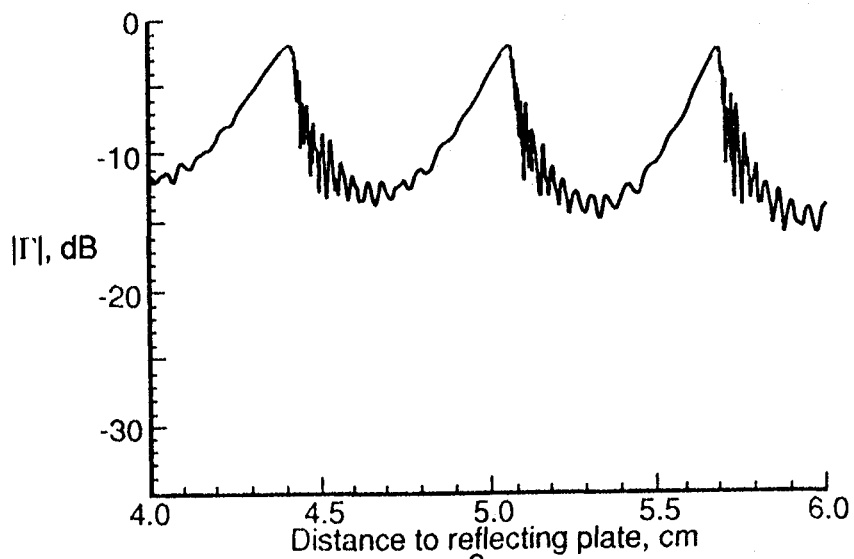


Figure 10. $|\Gamma|$ as a function of range for three-plate separation distances for a 2.57 cm diameter horn; with ground plane, without TPS tile, conical horn C, $\phi = 6^\circ$.

Conical horn B:

$\phi = 125^\circ$

With ground plane

With TPS tile

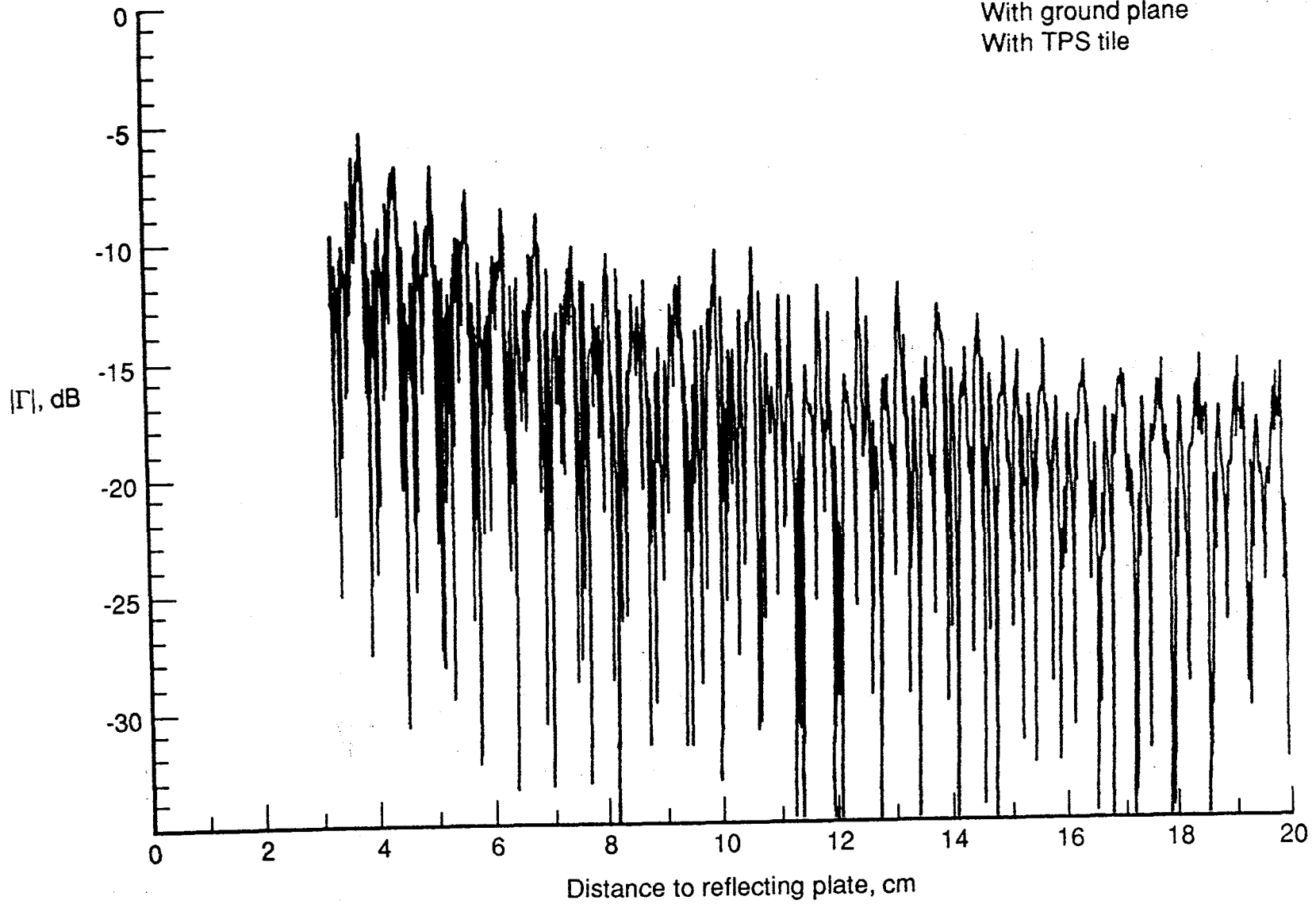


Figure 11. $|\Gamma|$ as a function of plate-separation distance for a 2.74 cm diameter horn.

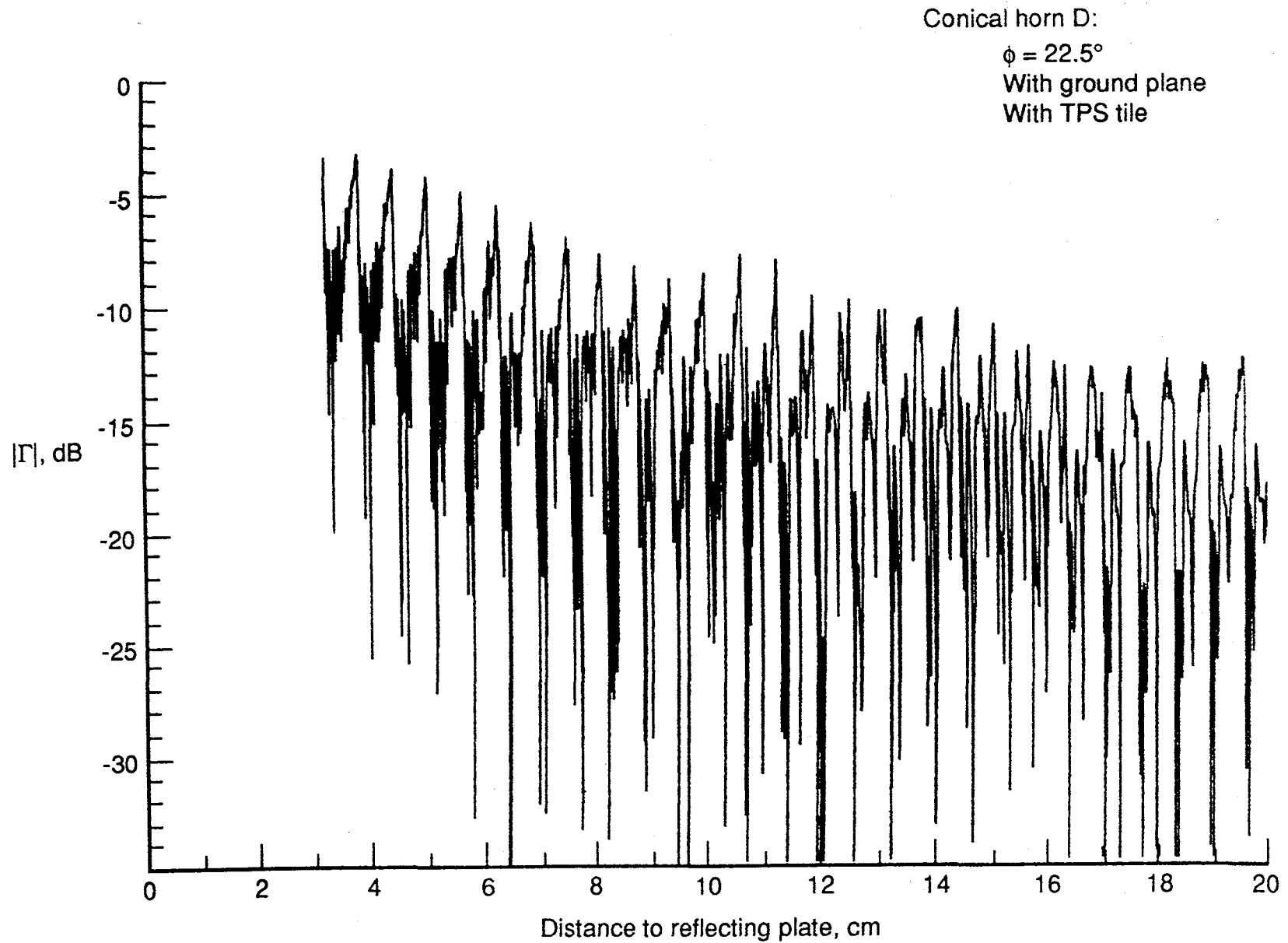


Figure 12. $|\Gamma|$ as a function of plate-separation distance for a 2.62 cm diameter horn.

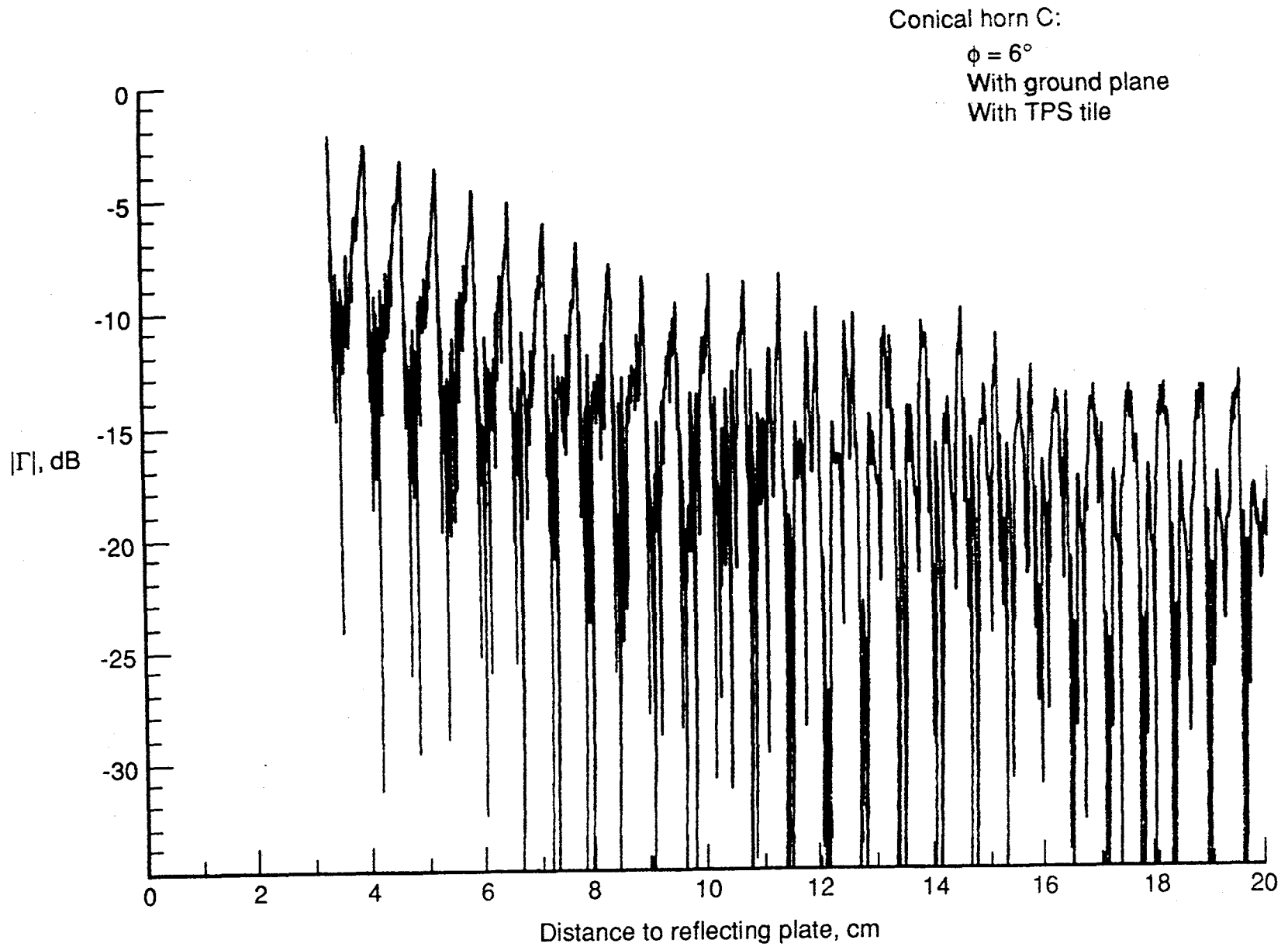


Figure 13. $|\Gamma|$ as a function of plate-separation distance for a 2.57 cm diameter horn.

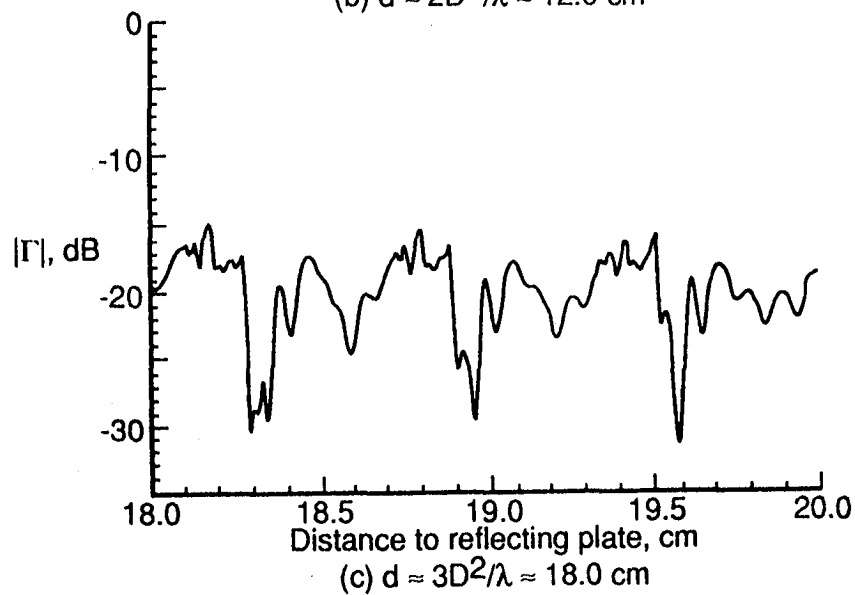
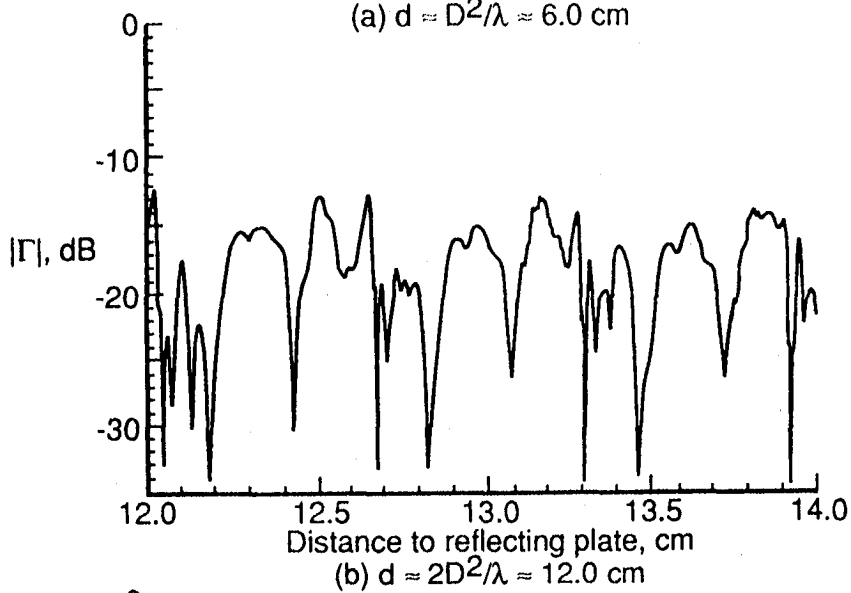
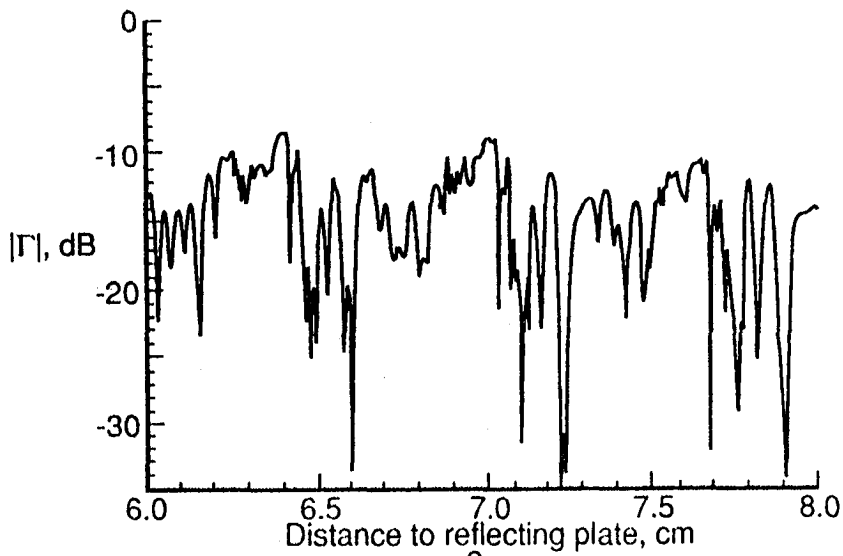


Figure 14. $|\Gamma|$ as a function of range for three plate-separation distances for a 2.74 cm diameter horn; with ground plane, with TPS tile, conical horn B, $\phi = 125^\circ$.

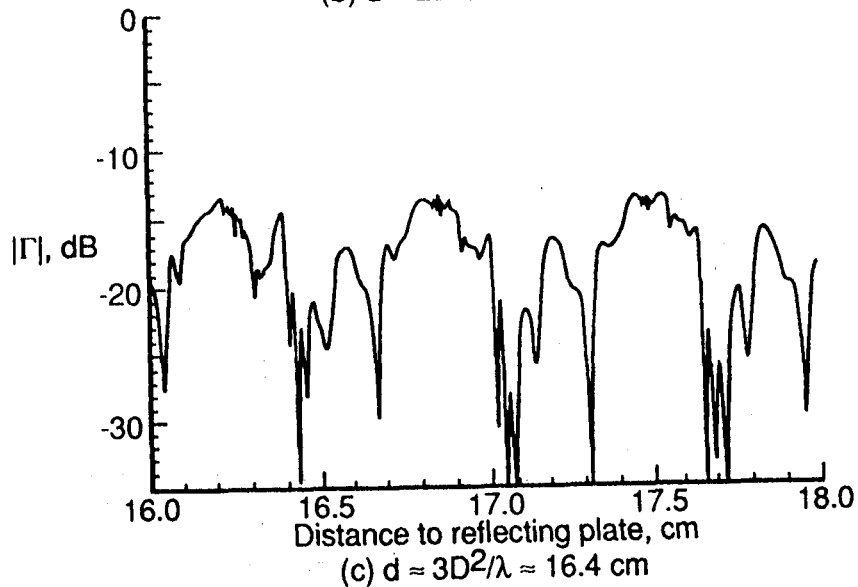
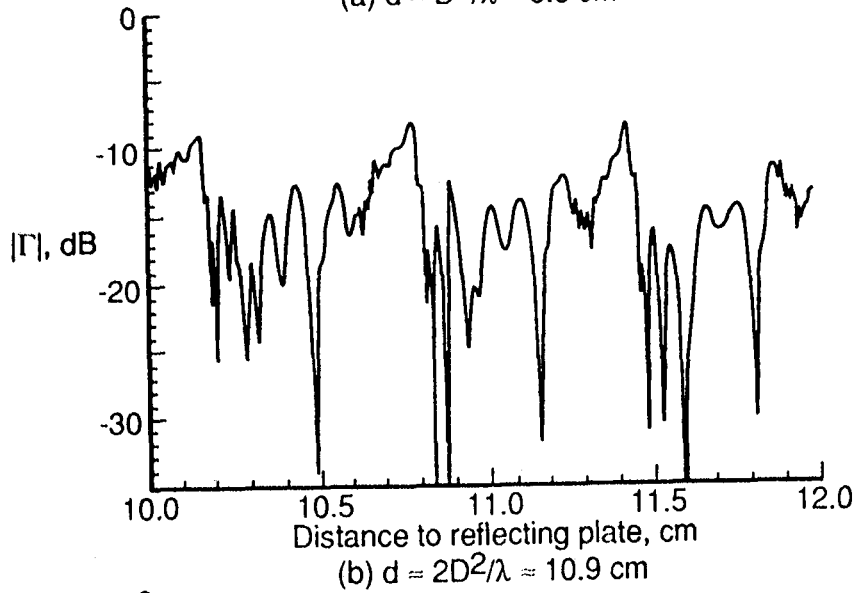
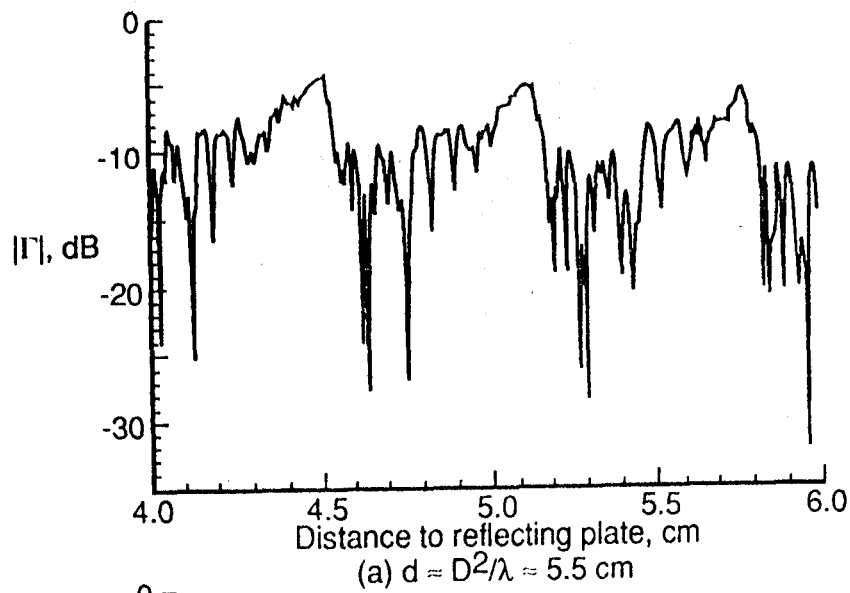


Figure 15. $|\Gamma|$ as a function of range for three plate-separation distances for a 2.62 cm diameter horn; with ground plane, with TPS tile, conical horn D , $\phi = 22.5^\circ$.

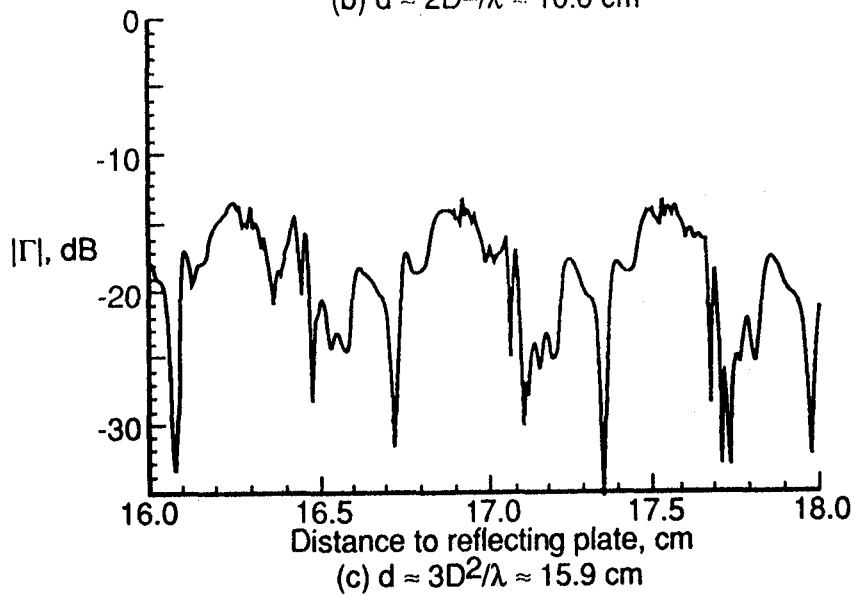
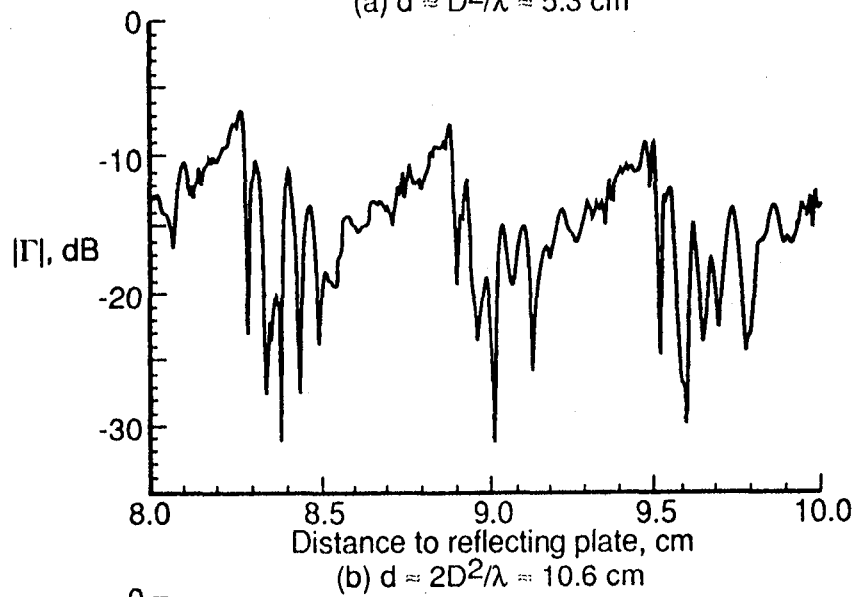
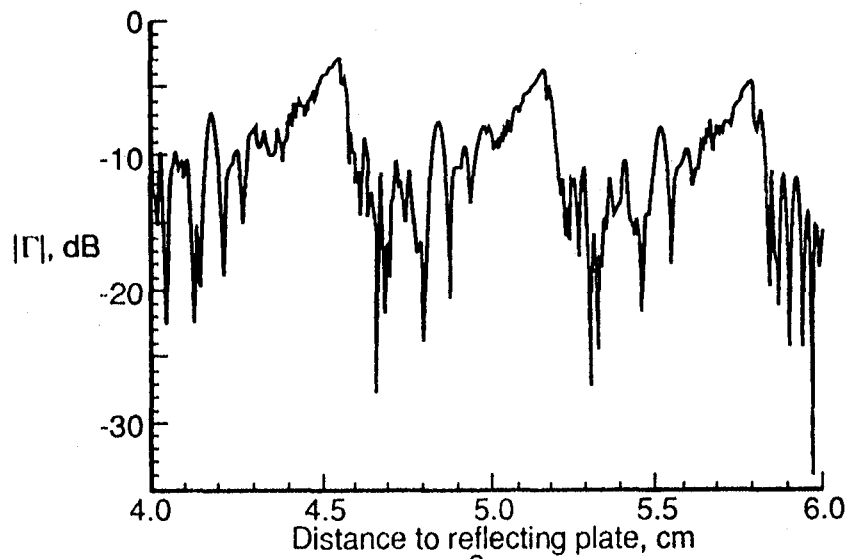


Figure 16. $|\Gamma|$ as a function of range for three plate-separation distances for a 2.57 cm diameter horn; with ground plane, with TPS tile, conical horn C, $\phi = 6^\circ$.

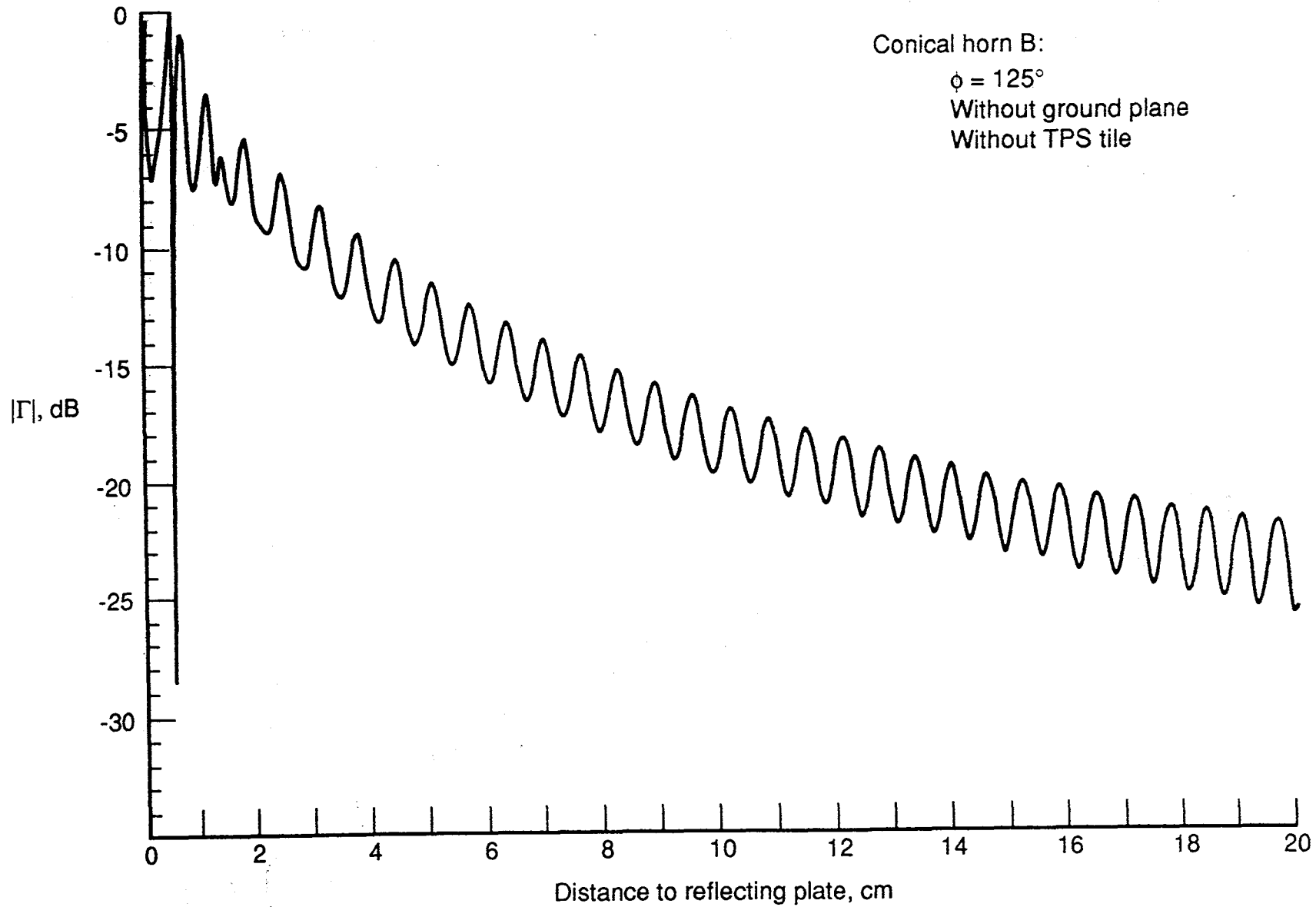


Figure 17. $|\Gamma|$ as a function of separation distance between the antenna-aperture plane and a reflecting plate for a 2.54 cm diameter horn.

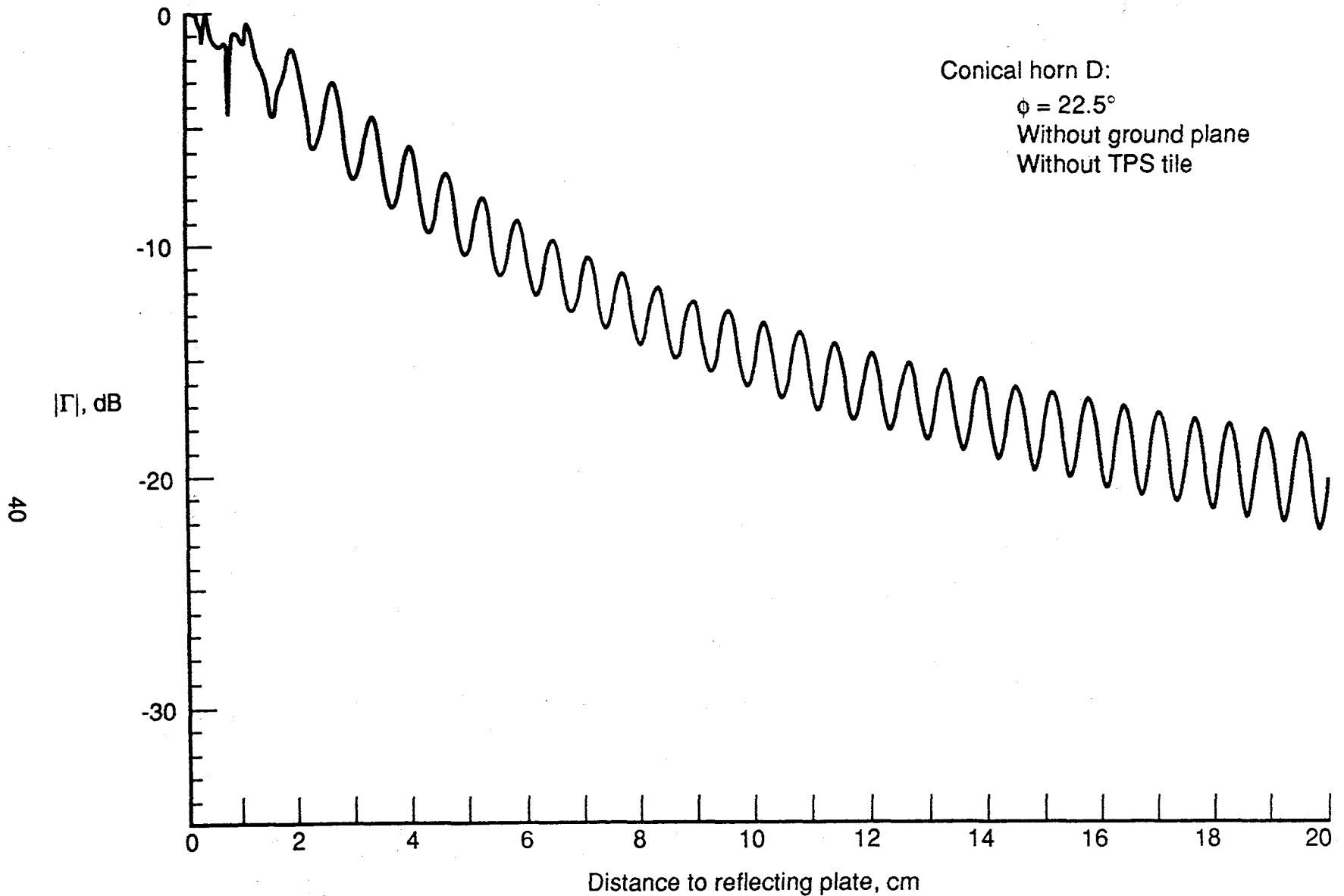


Figure 18. $|\Gamma|$ as a function of separation distance between the antenna-aperture plane and a reflecting plate for a 2.54 cm diameter horn.

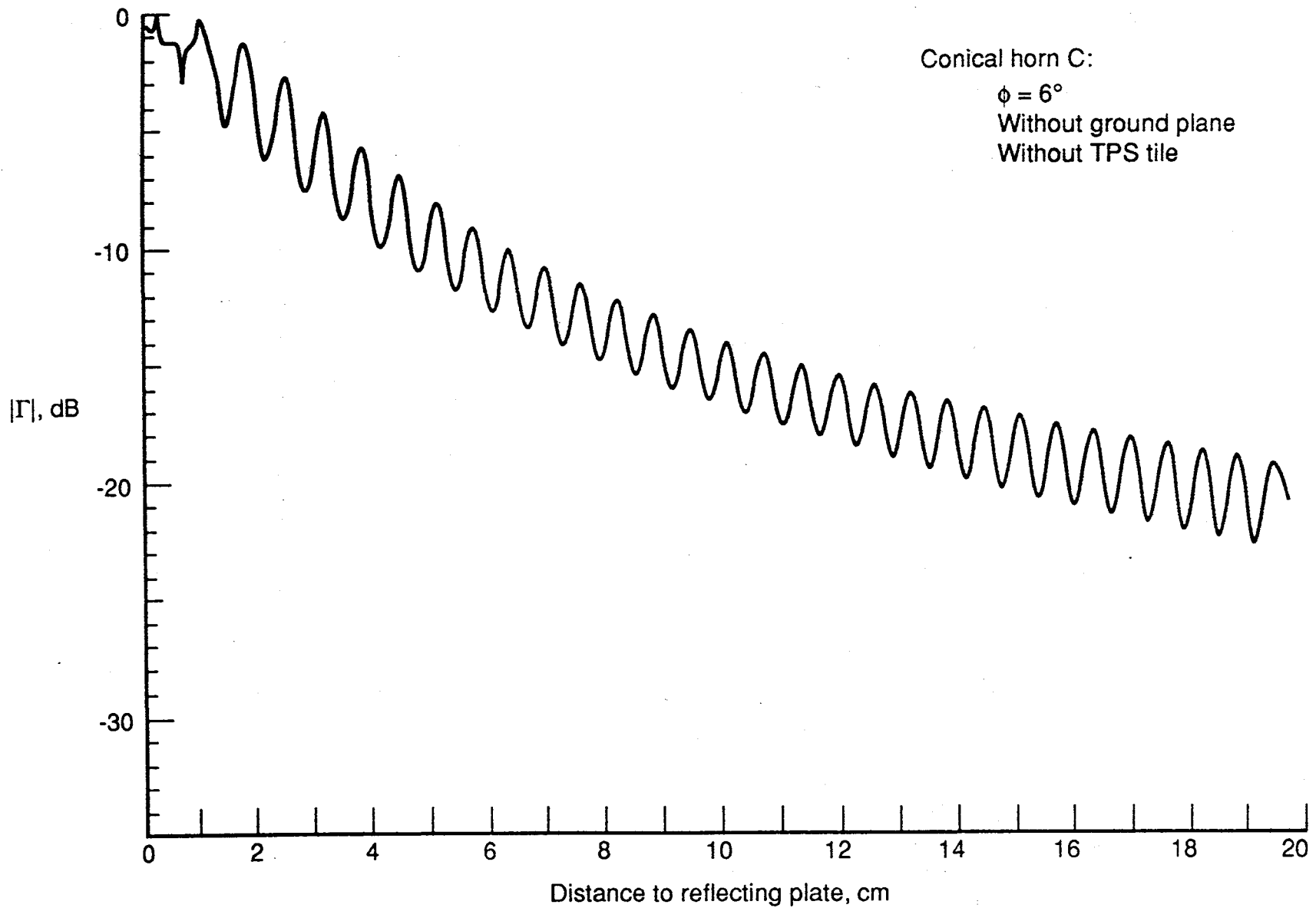


Figure 19. $|\Gamma|$ as a function of separation distance between the antenna-aperture plane and a reflecting plate for a 2.54 cm diameter horn.

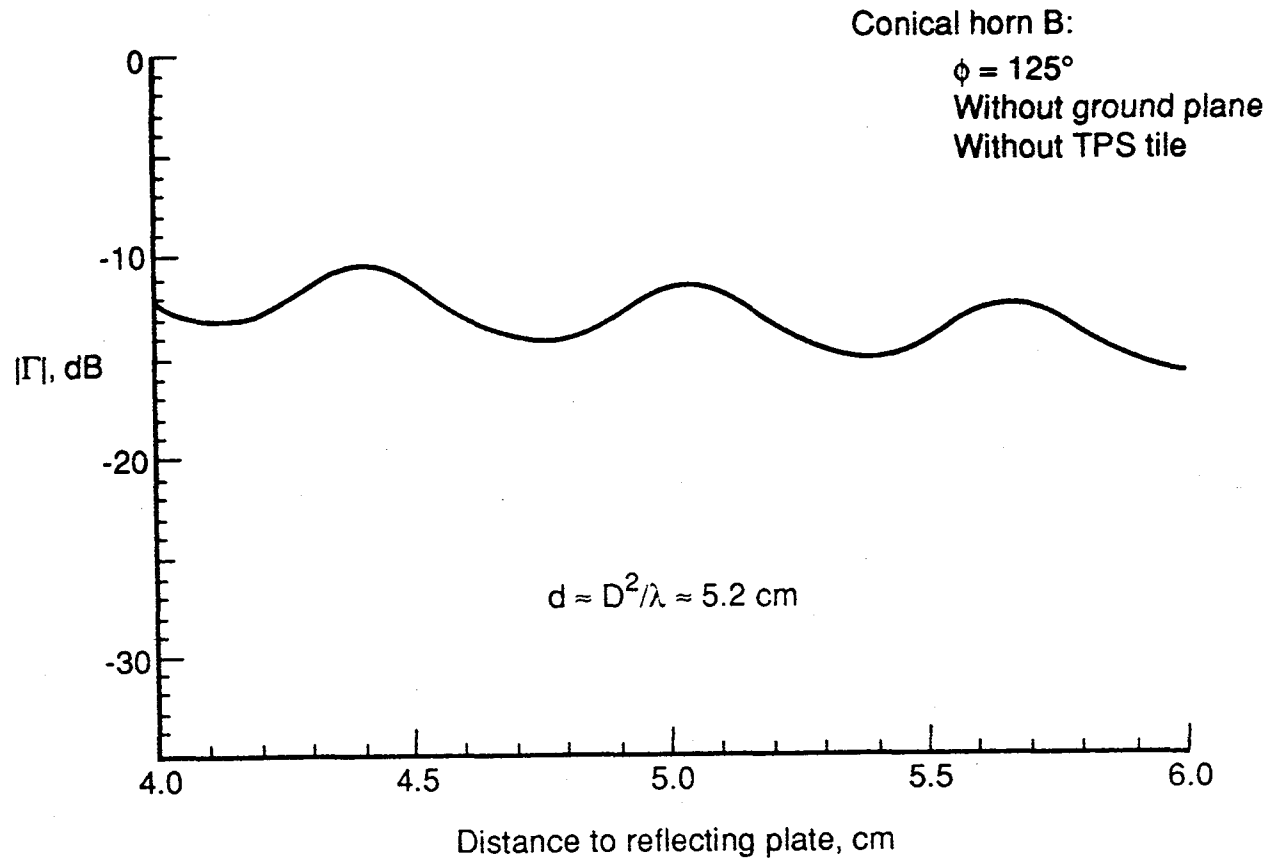


Figure 20. $|\Gamma|$ as a function of separation distance between the antenna-aperture plane and a reflecting plate for a 2.54 cm diameter horn.

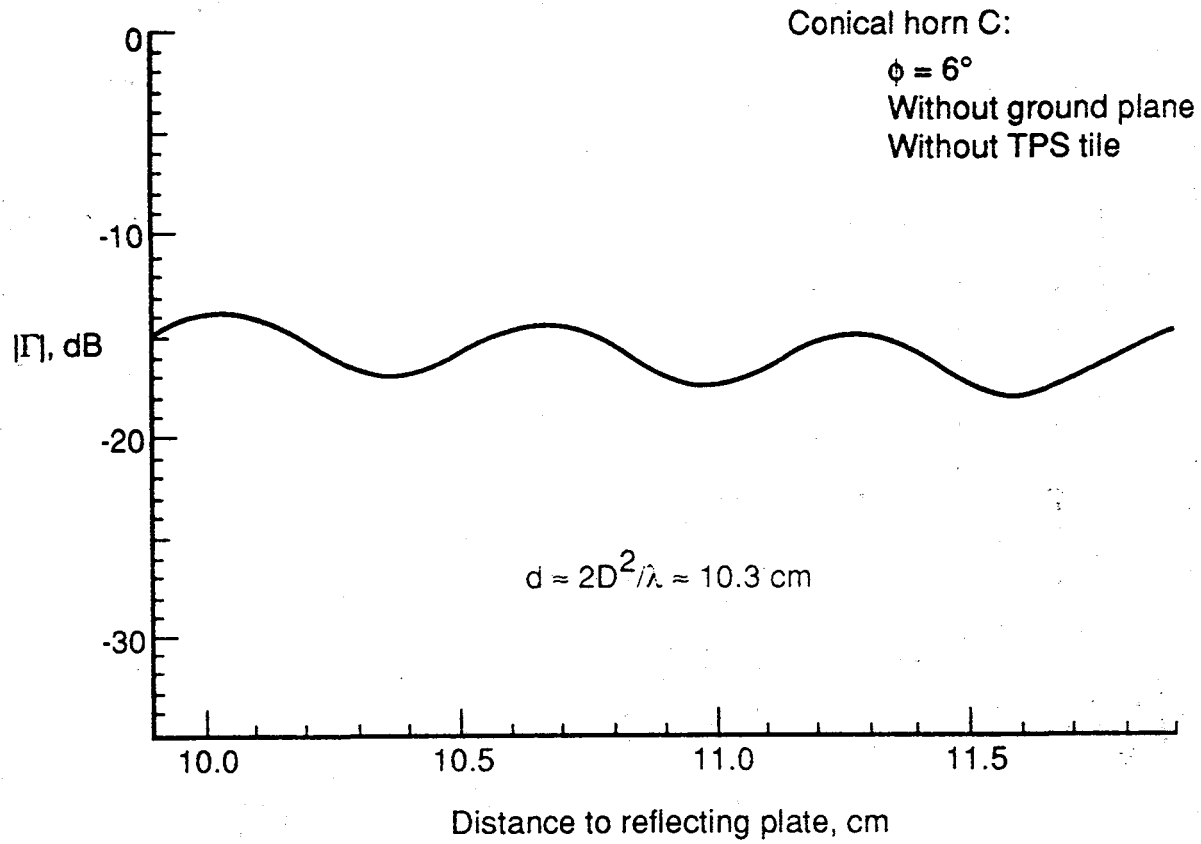


Figure 21. $|\Gamma|$ as a function of separation distance between the antenna-aperture plane and a reflecting plate for a 2.54 cm diameter horn.

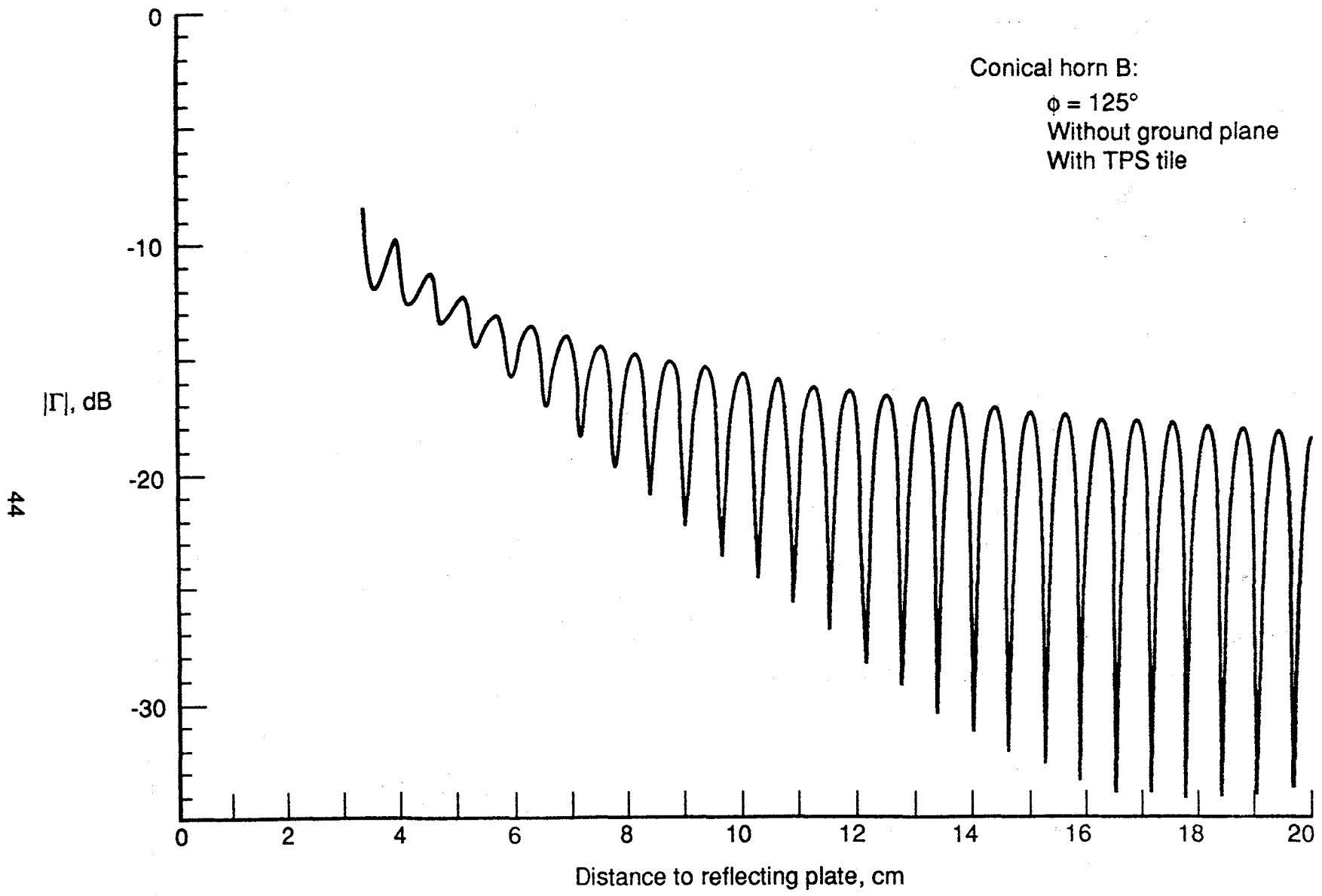


Figure 22. $|\Gamma|$ as a function of separation distance between the antenna-aperture plane and a reflecting plate for a 2.54 cm diameter horn.

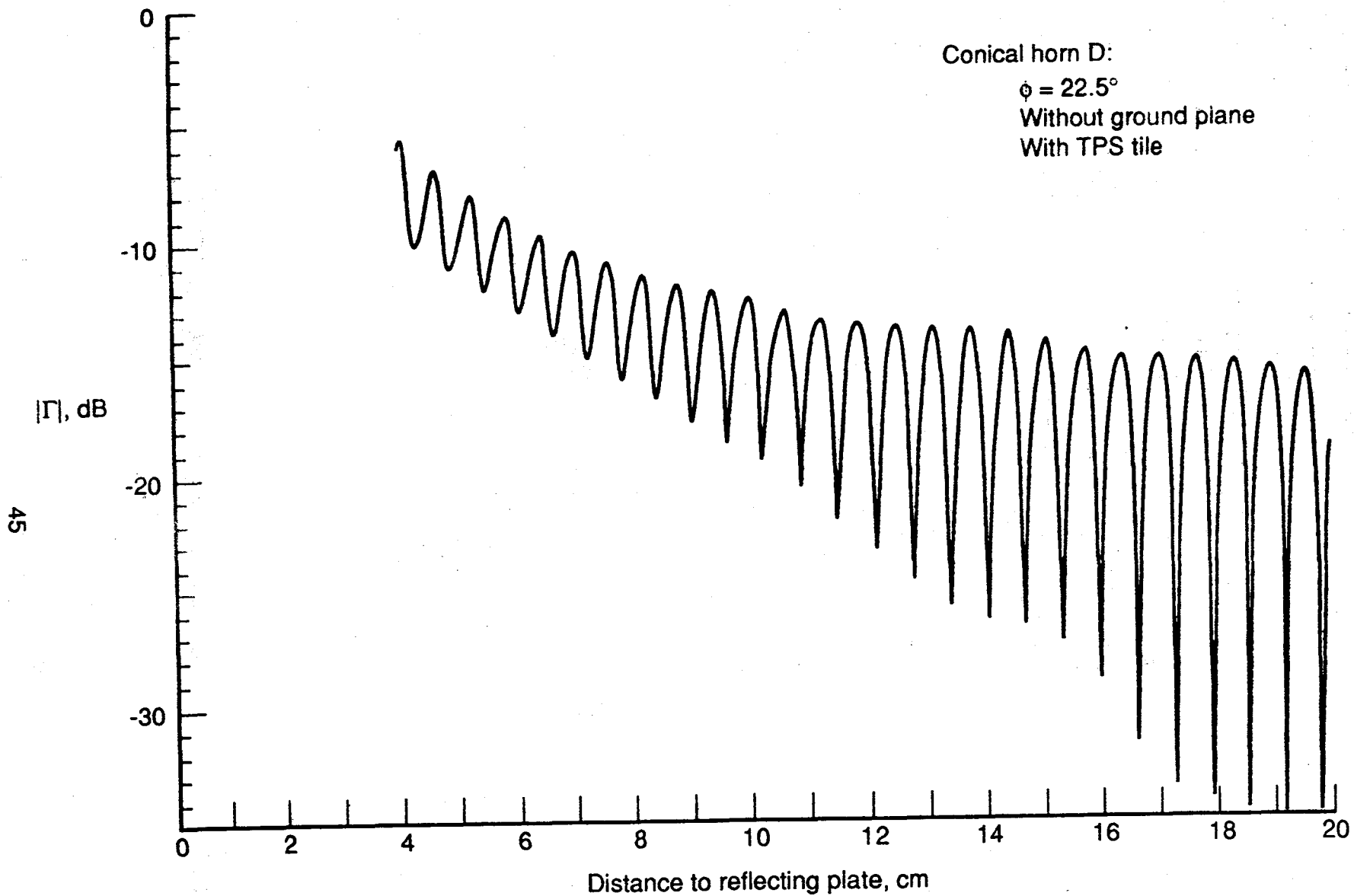


Figure 23. $|\Gamma|$ as a function of separation distance between the antenna-aperture plane and a reflecting plate for a 2.54 cm diameter horn.

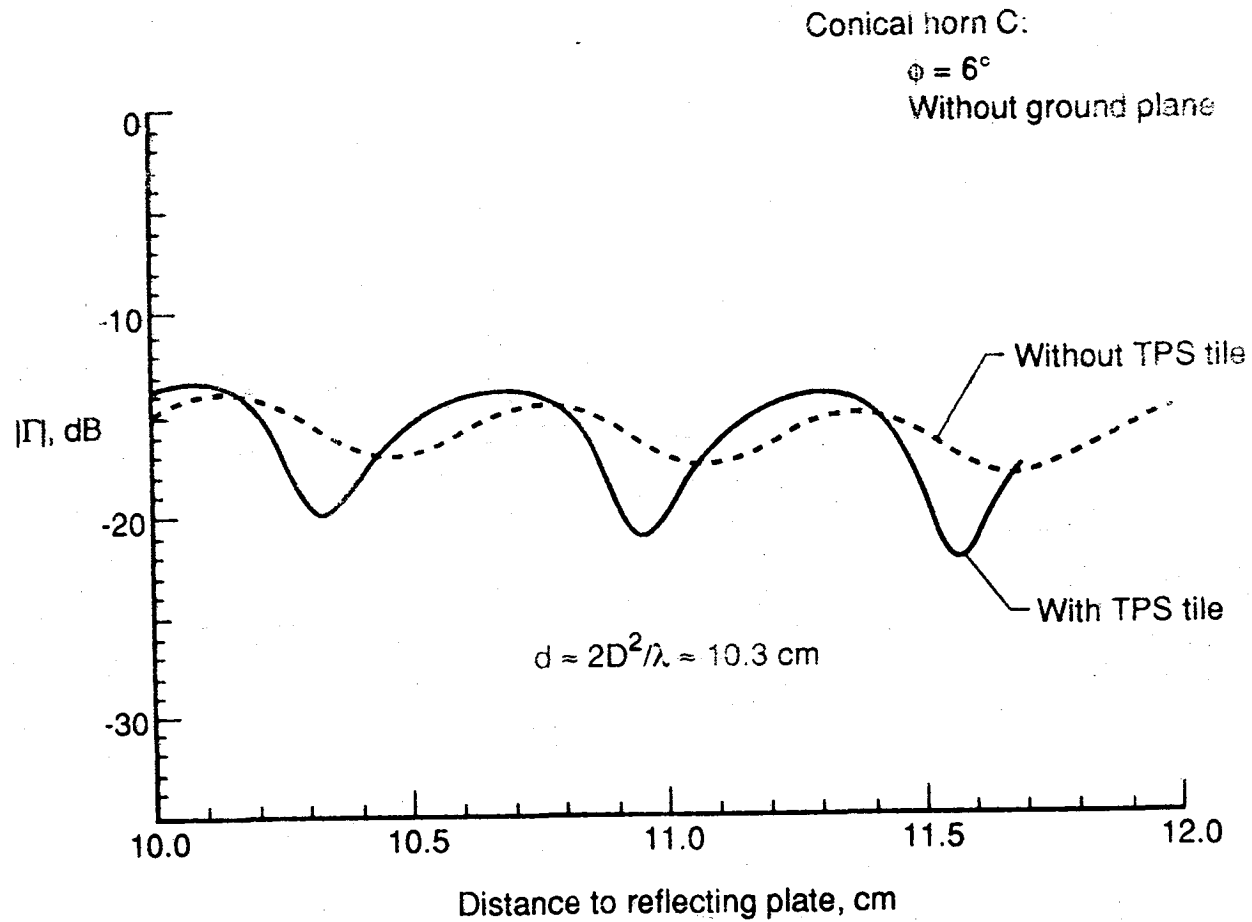


Figure 25. $|\Gamma|$ as a function of separation distance between the antenna-aperture plane and a reflecting plate for a 2.54 cm diameter horn.

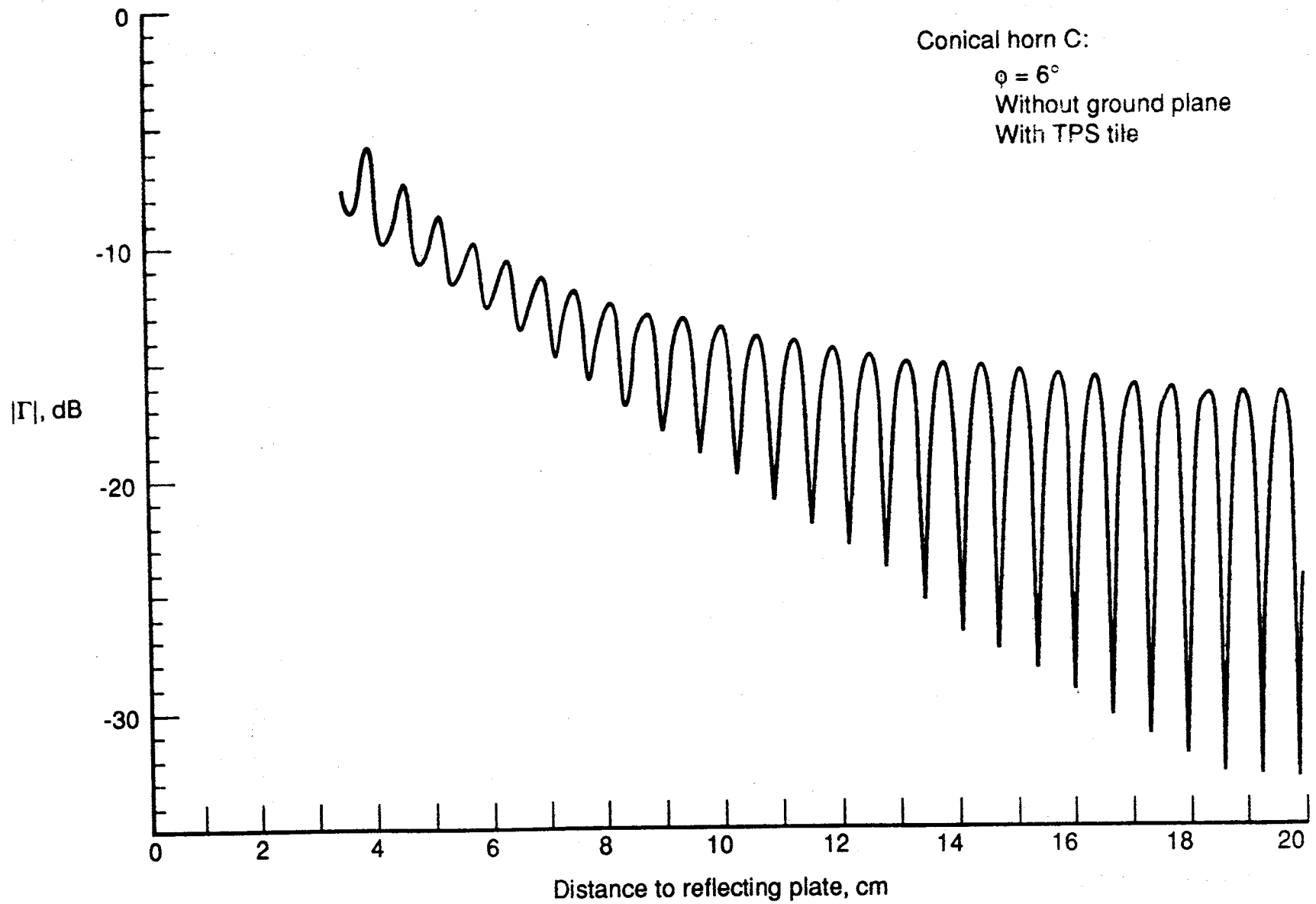


Figure 24. $|\Gamma|$ as a function of separation distance between the antenna-aperture plane and a reflecting plate for a 2.54 cm diameter horn.

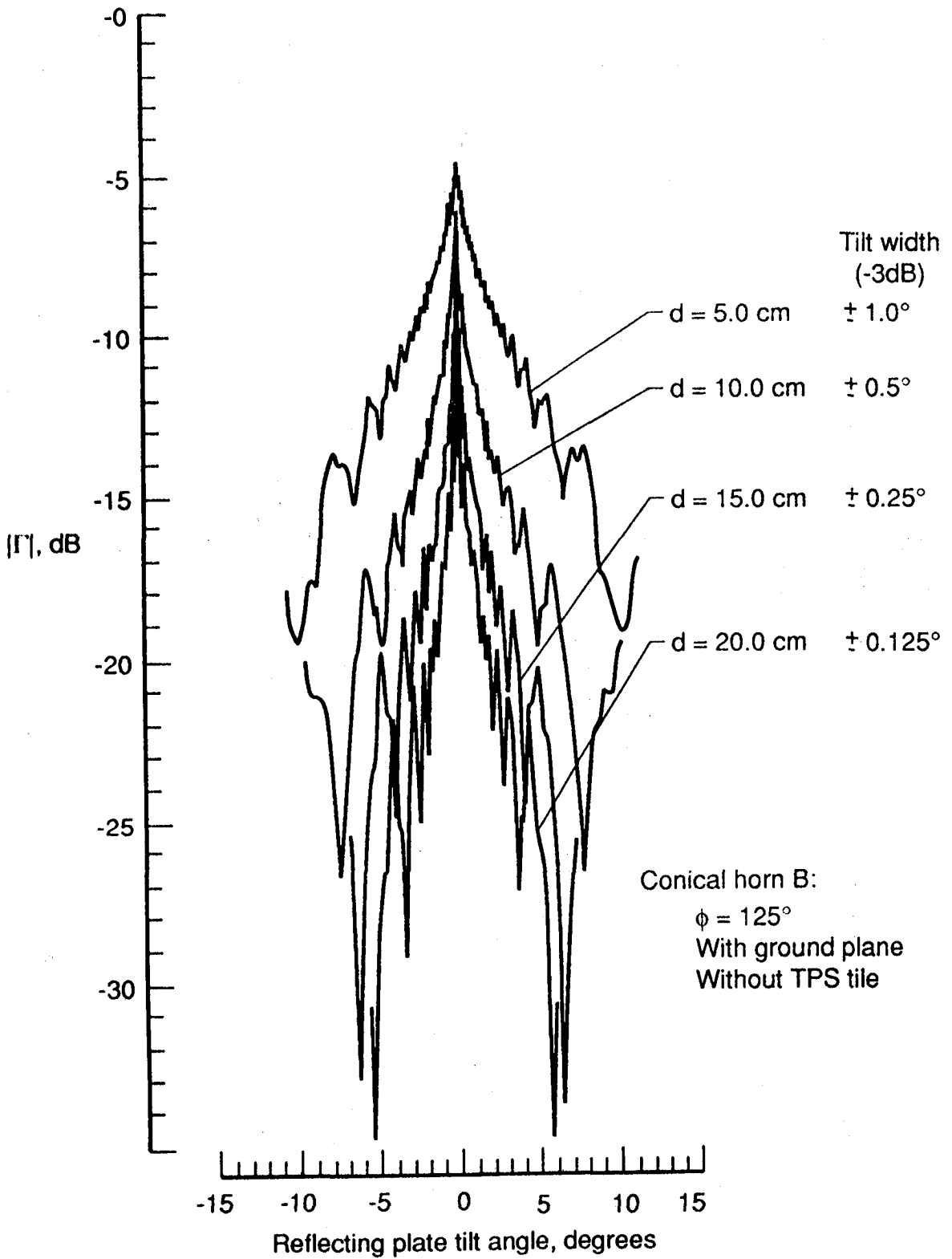


Figure 26. $|\Gamma|$ as a function of reflecting plate tilt angle for four plate-separation distances for a 2.74 cm diameter horn.

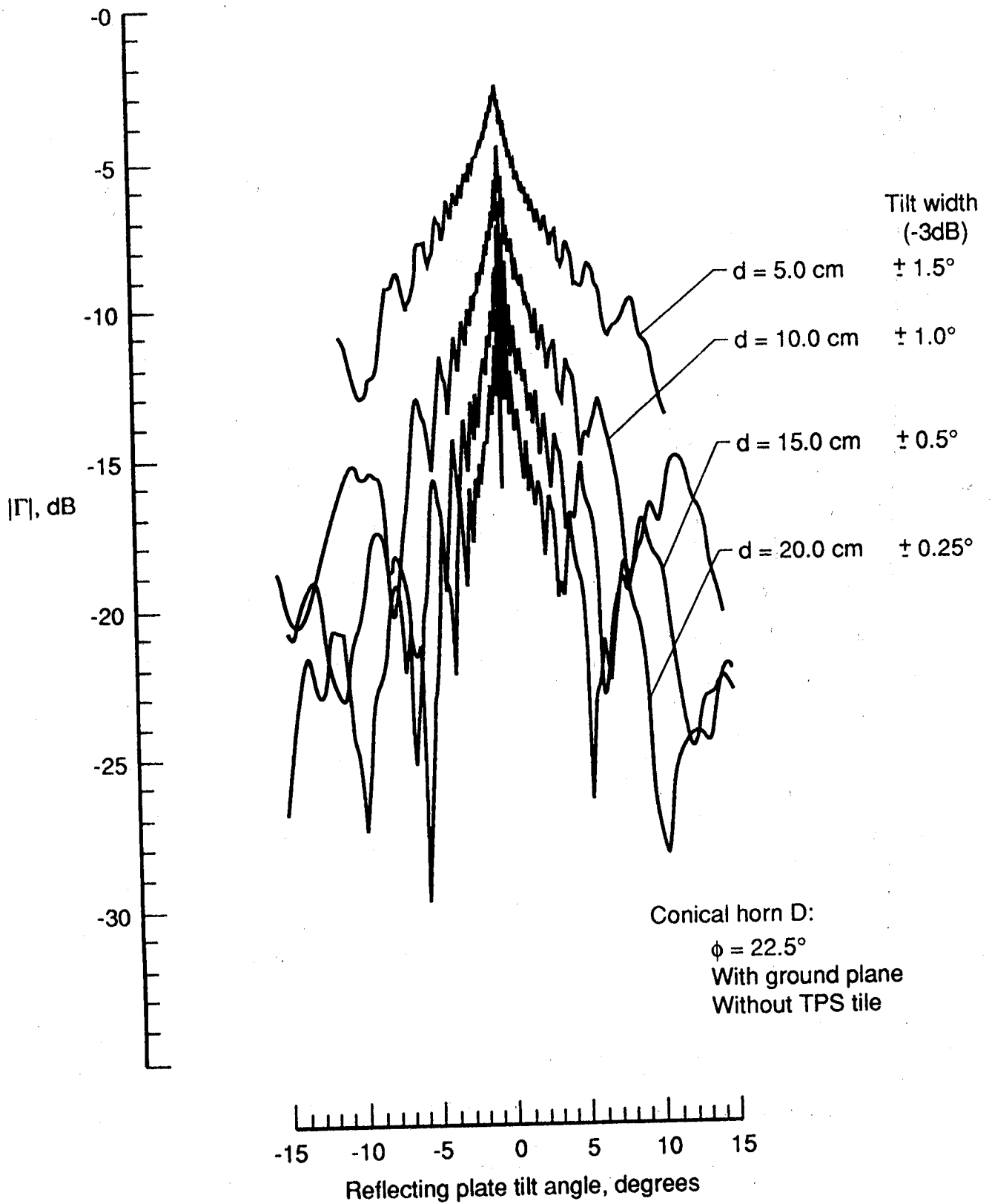


Figure 27. $|\Gamma|$ as a function of reflecting plate tilt angle for four plate-separation distances for a 2.62 cm diameter horn.

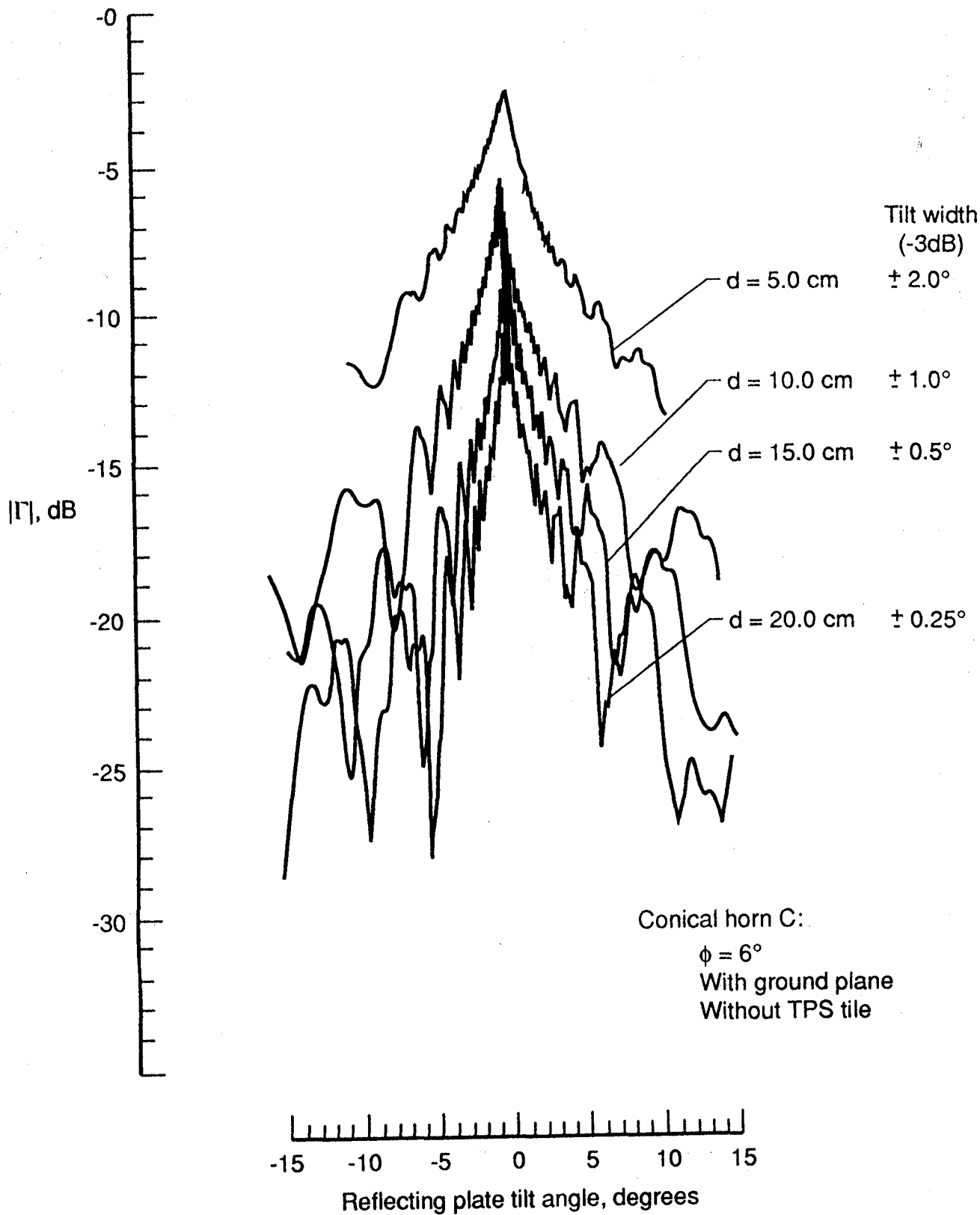


Figure 28. $|\Gamma|$ as a function of reflecting plate tilt angle for four plate-separation distances for a 2.57 cm diameter horn.

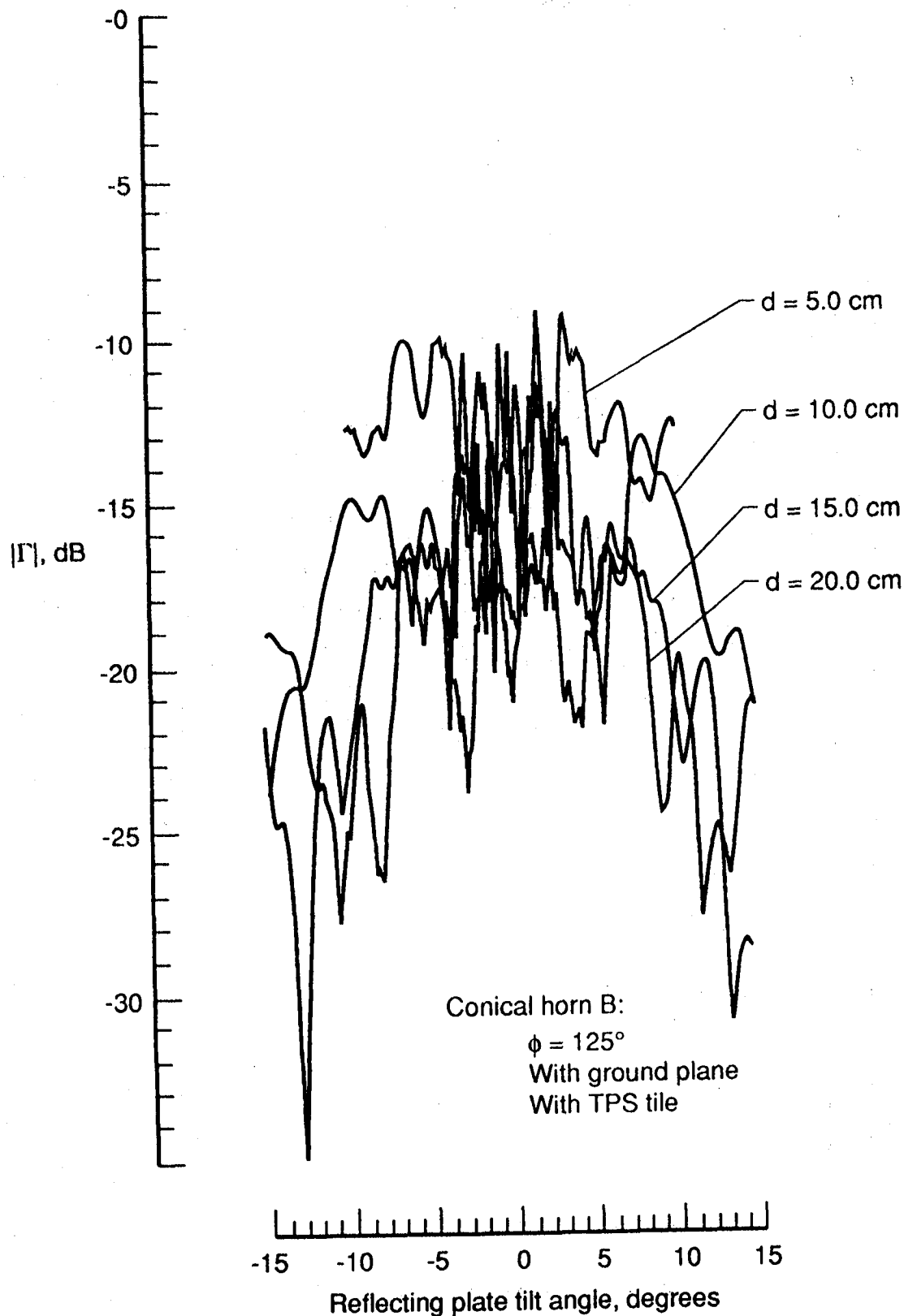


Figure 29. $|\Gamma|$ as a function of reflecting plate tilt angle for four plate-separation distances for a 2.74 cm diameter horn.

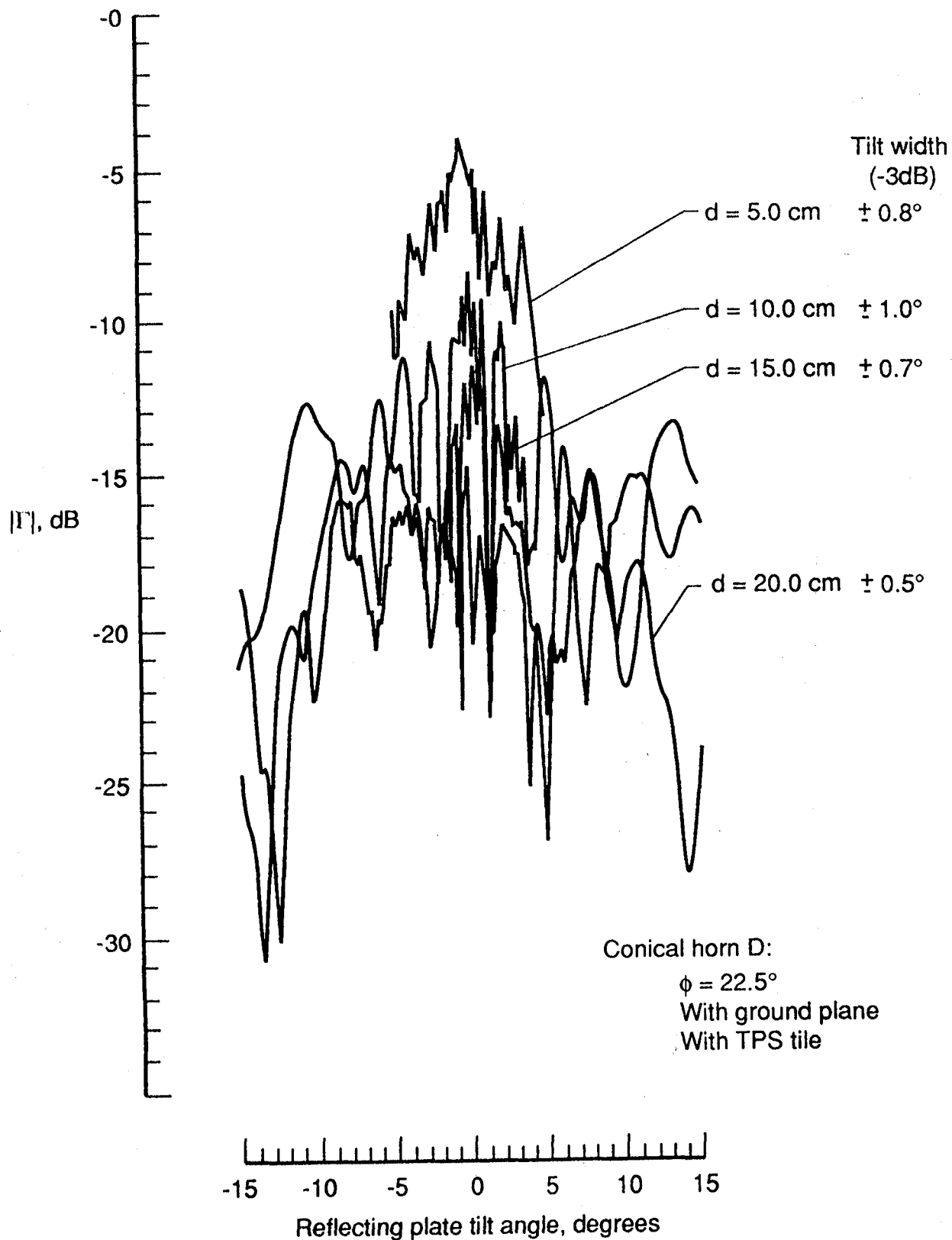


Figure 30. $|\Gamma|$ as a function of reflecting plate tilt angle for four plate-separation distances for a 2.62 cm diameter horn.

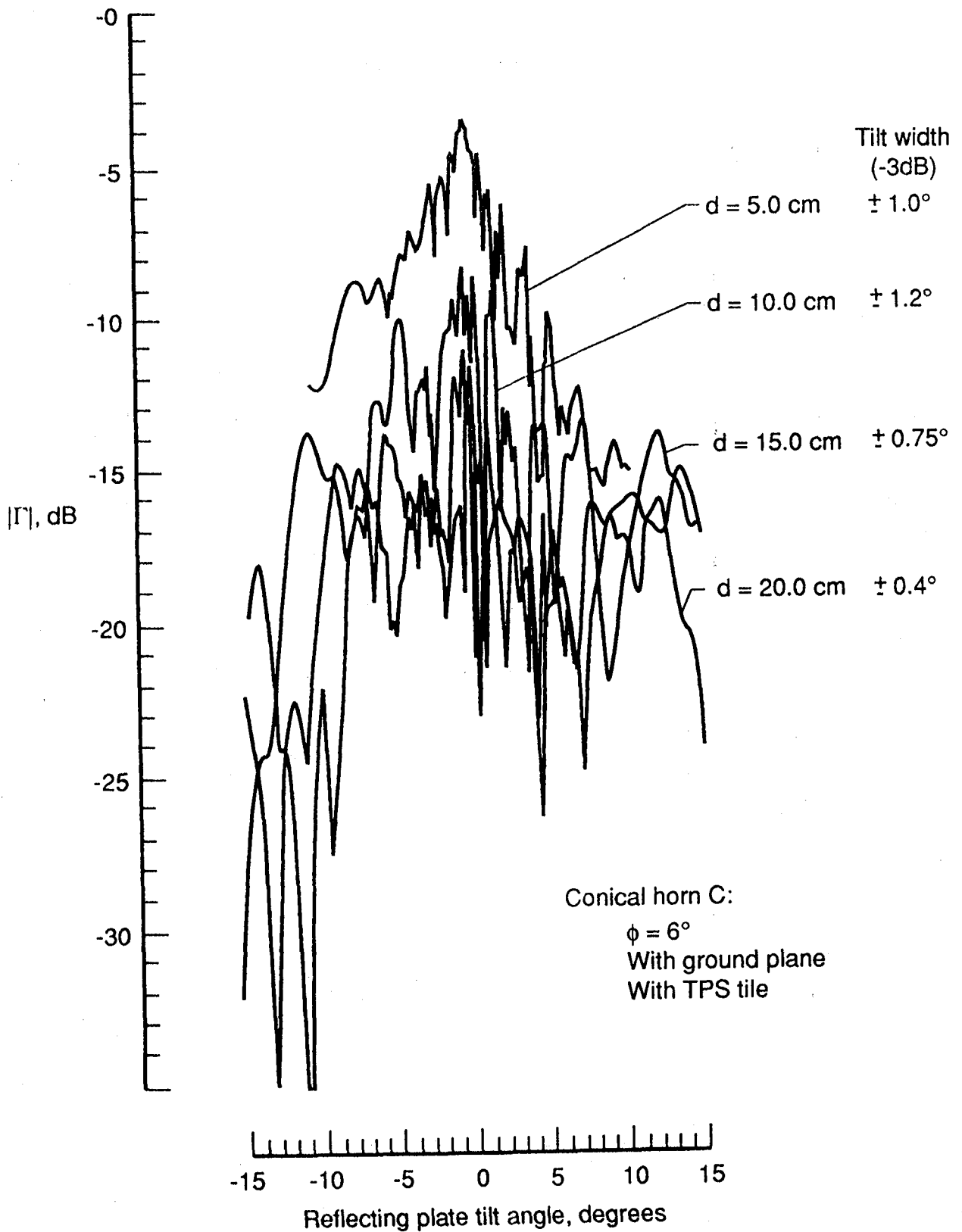


Figure 31. $|\Gamma|$ as a function of reflecting plate tilt angle for four plate-separation distances for a 2.57 cm diameter horn.

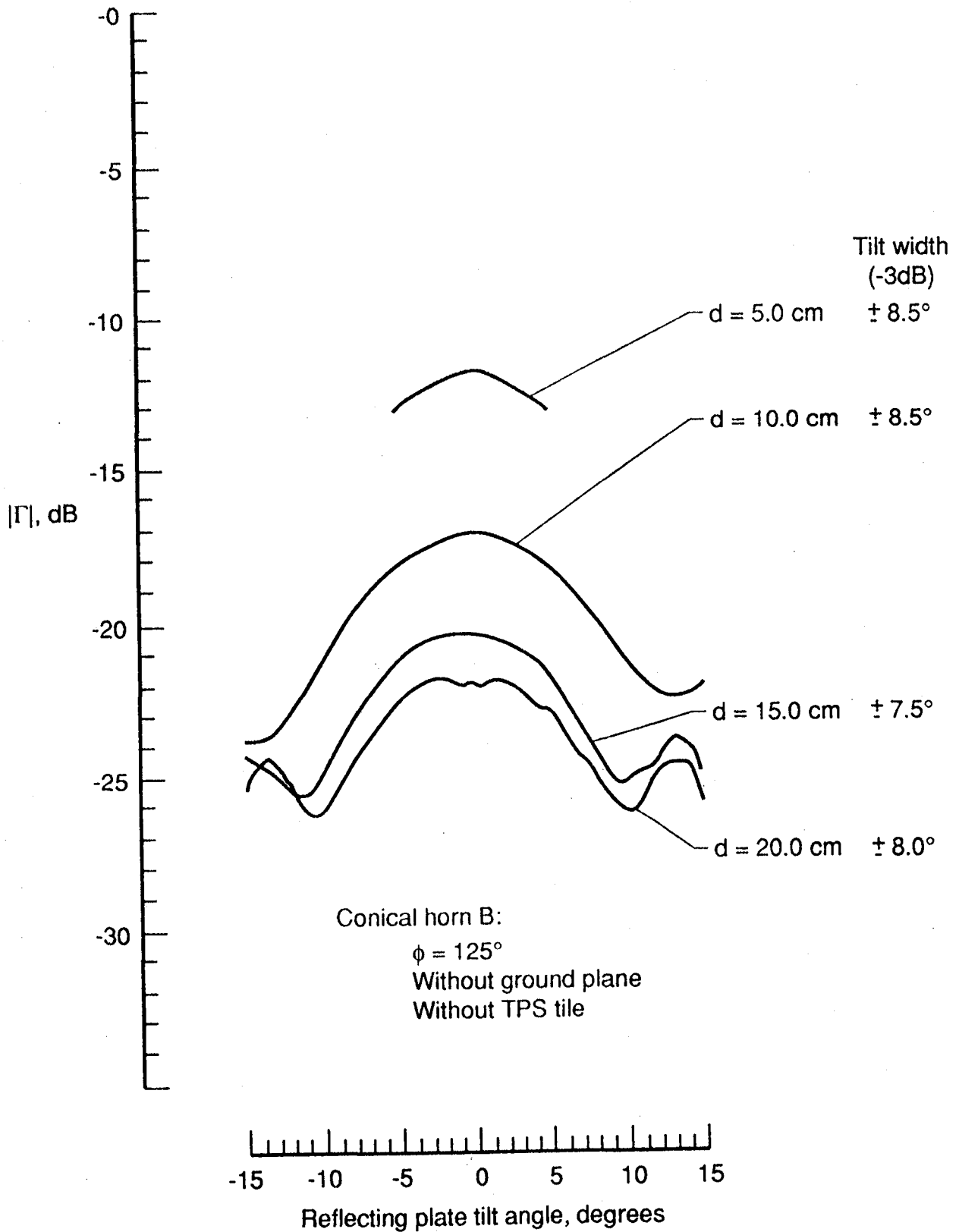


Figure 32. $|\Gamma|$ as a function of reflecting plate tilt angle for four aperture-plane to reflecting-plate separation distances for a 2.54 cm diameter horn.

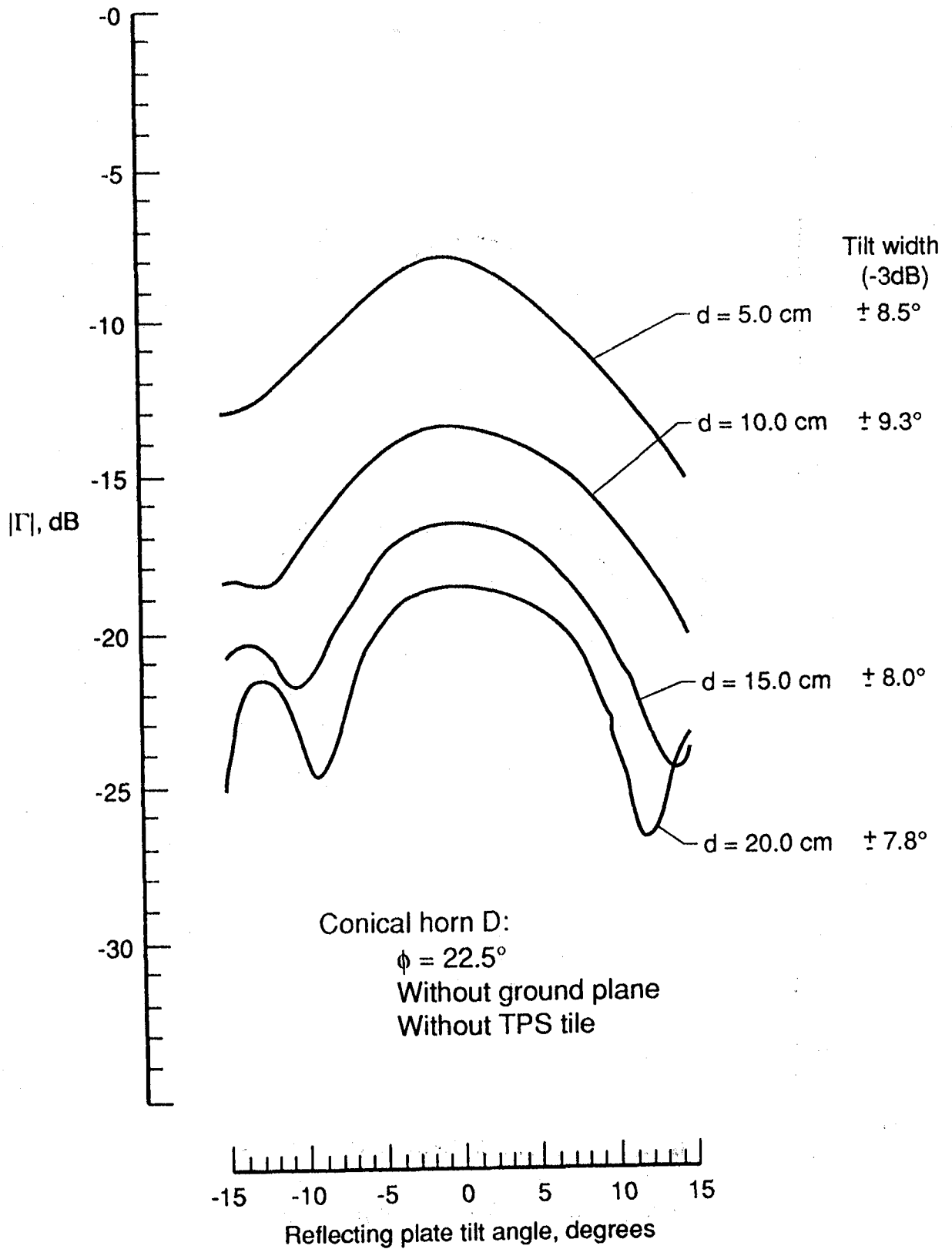


Figure 33. $|\Gamma|$ as a function of reflecting plate tilt angle for four aperture-plane to reflecting-plate separation distances for a 2.54 cm diameter horn.

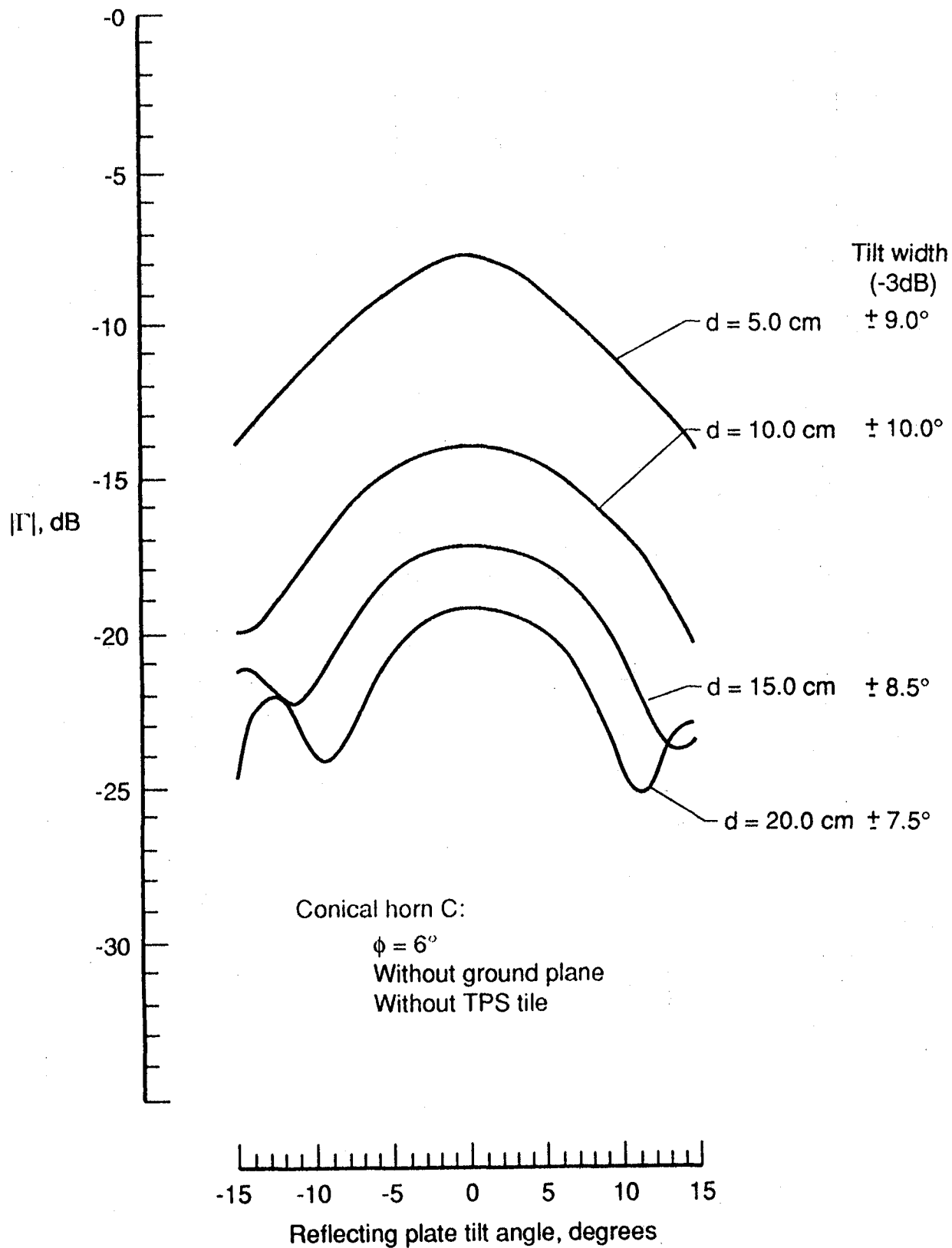


Figure 34. $|\Gamma|$ as a function of reflecting plate tilt angle for four aperture-plane to reflecting-plate separation distances for a 2.54 cm diameter horn.

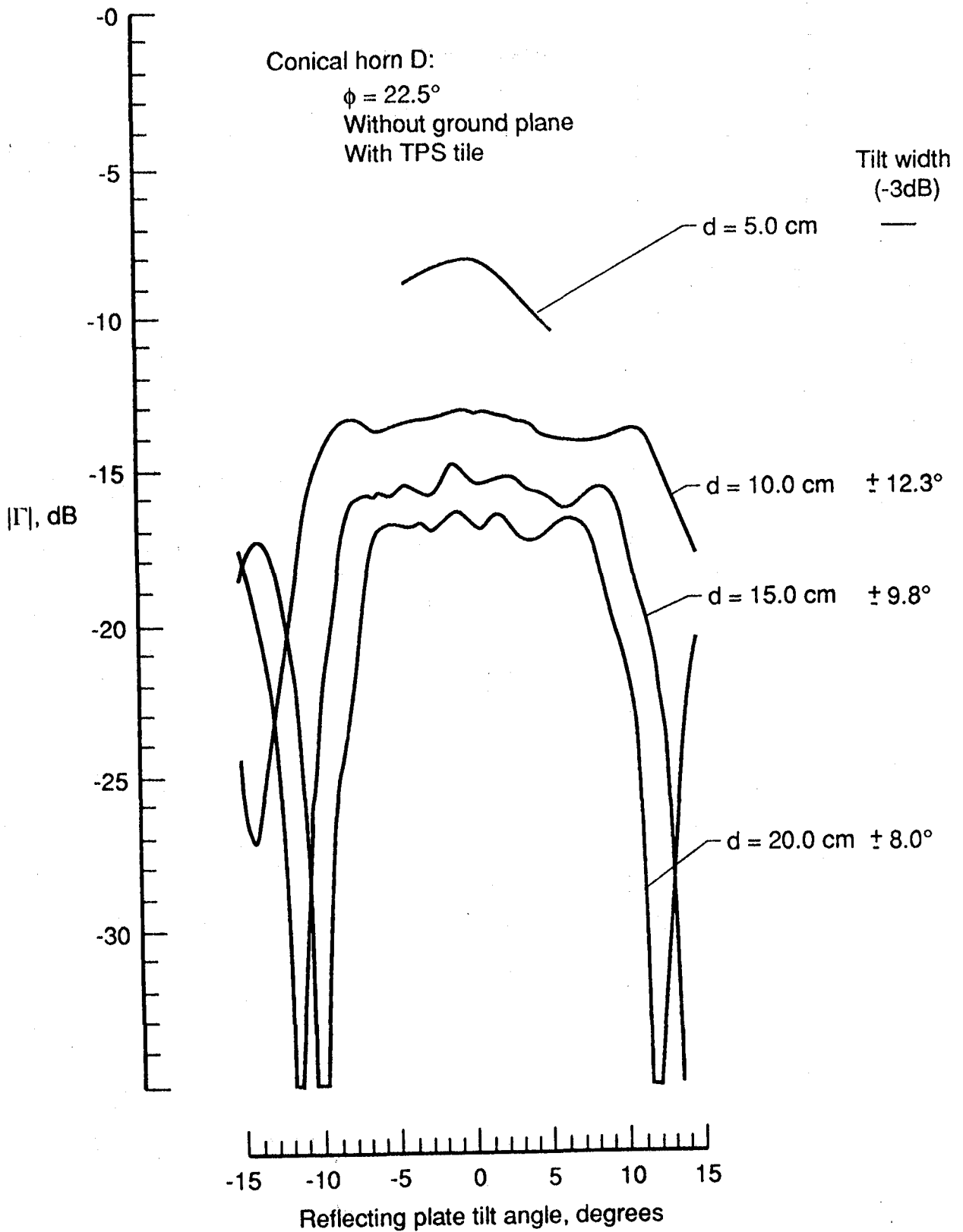


Figure 35. $|\Gamma|$ as a function of reflecting plate tilt angle for four aperture-plane to reflecting-plate separation distances for a 2.54 cm diameter horn.

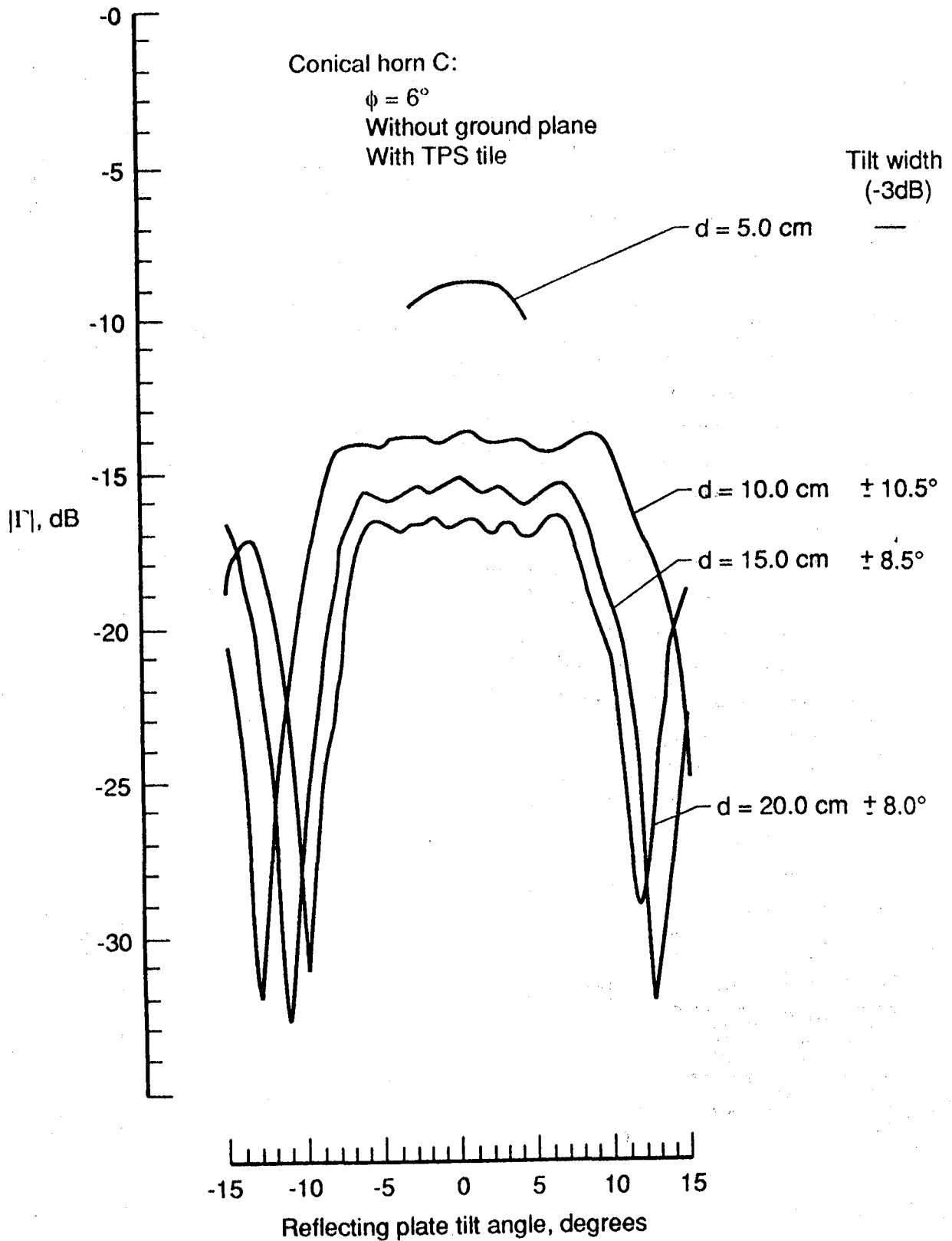


Figure 36. $|\Gamma|$ as a function of reflecting plate tilt angle for four aperture-plane to reflecting-plate separation distances for a 2.54 cm diameter horn.

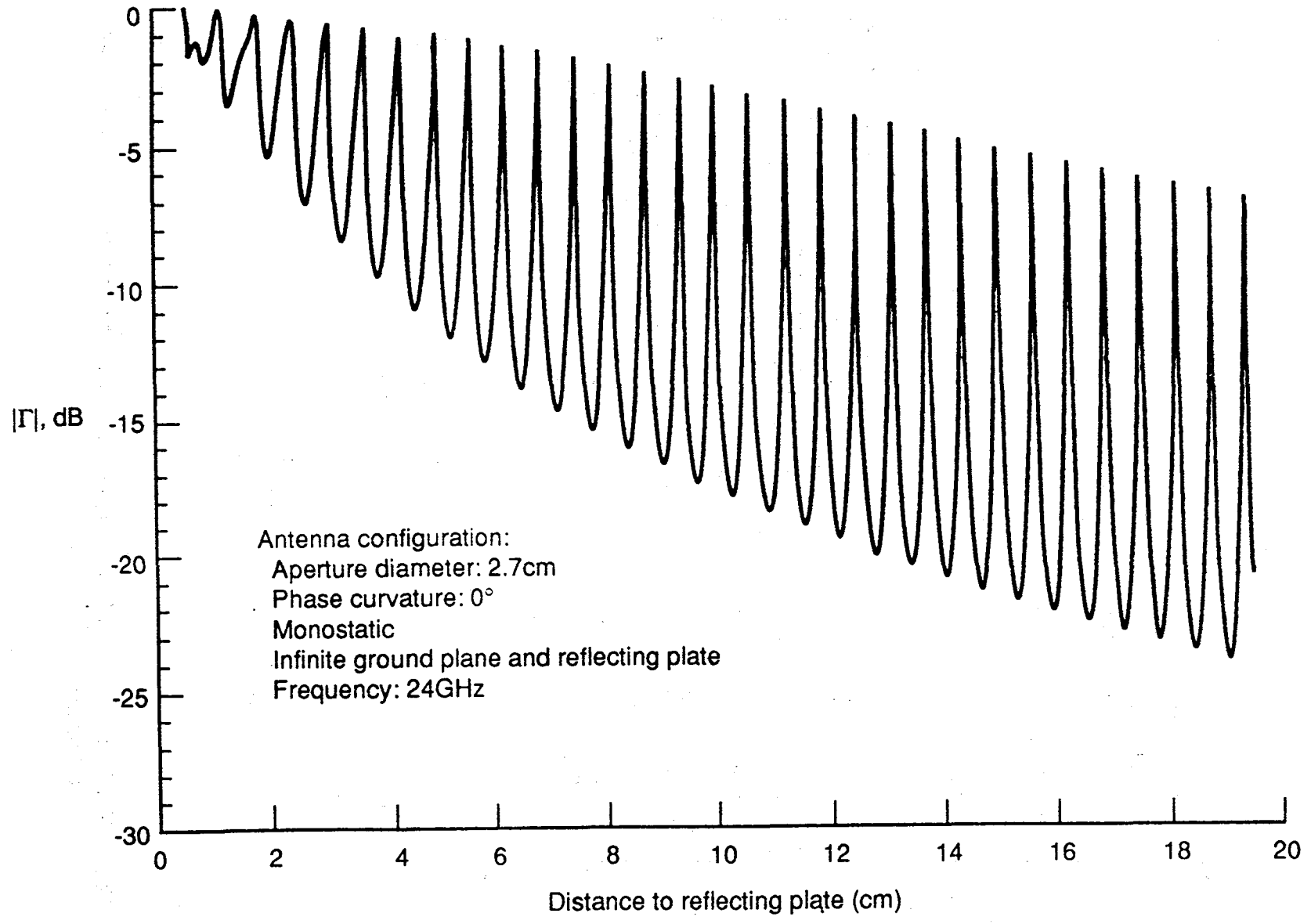


Figure 37. CWG model, reflection coefficient prediction.

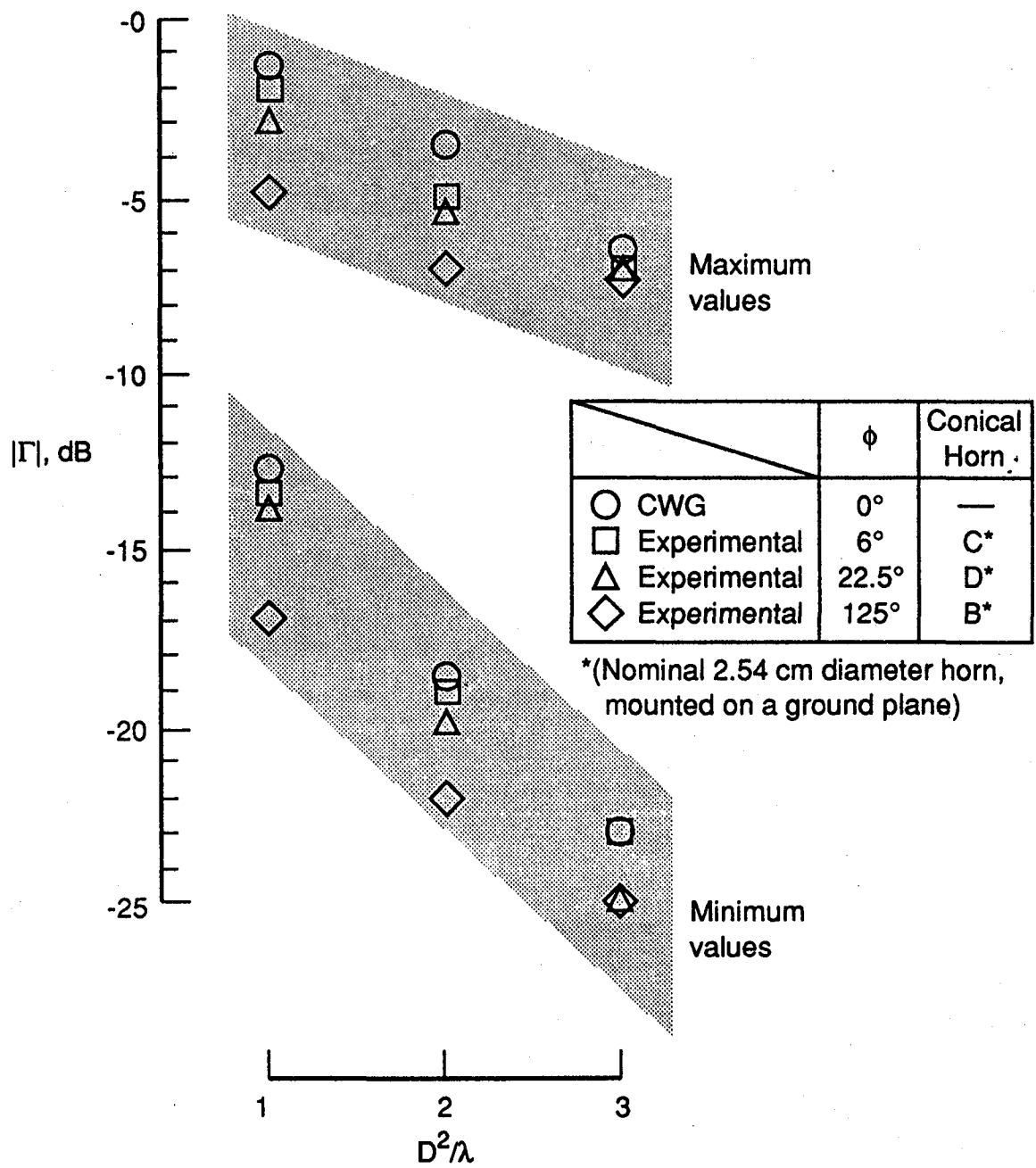
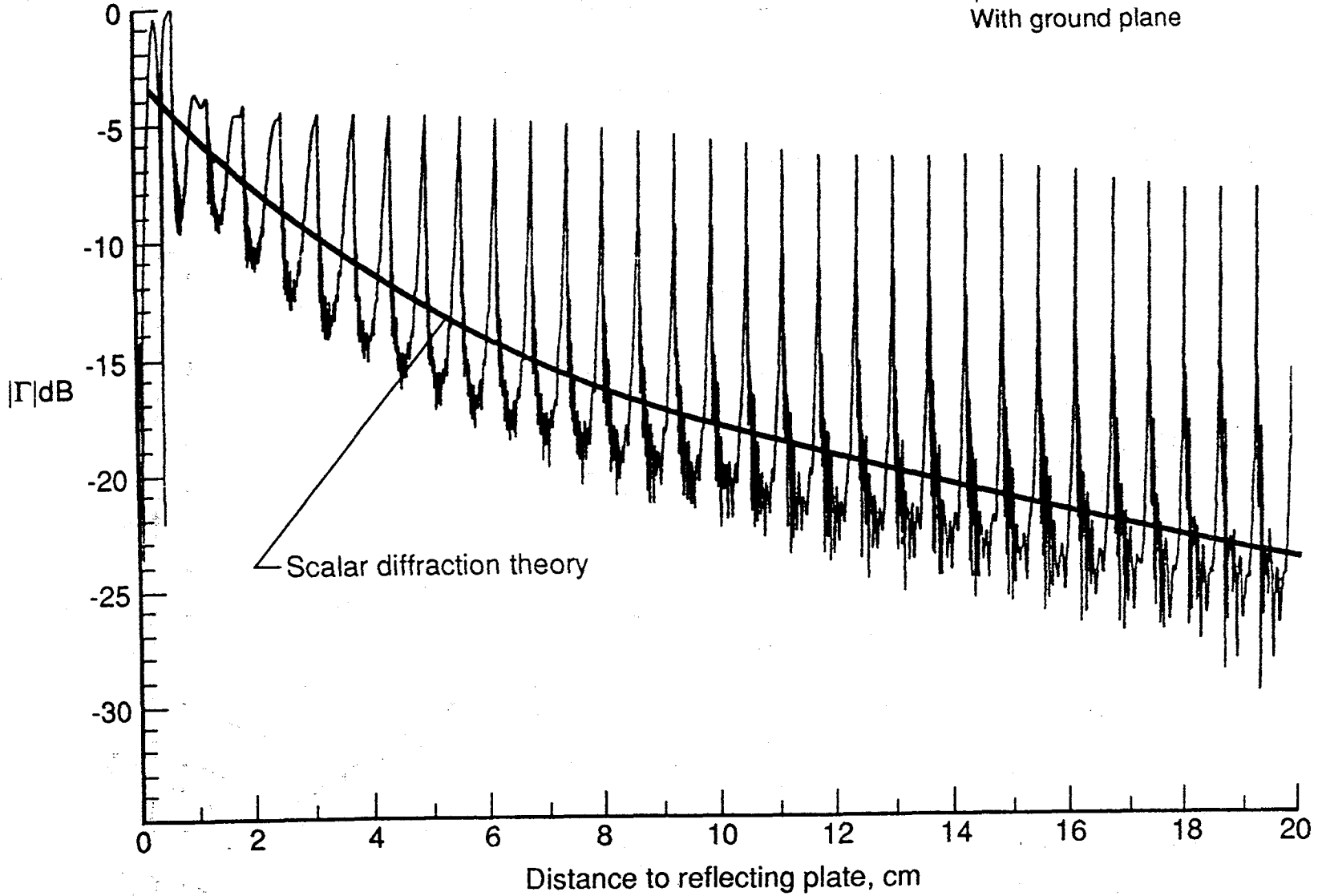


Figure 38. Comparison of $|\Gamma|$ between the experimental data and the CWG model for 2.2λ aperture antennas.

Conical horn B:
 $\phi = 125^\circ$
With ground plane



61

Figure 39. Comparison of scalar diffraction theory predictions with measurements from a 2.74 cm diameter horn.

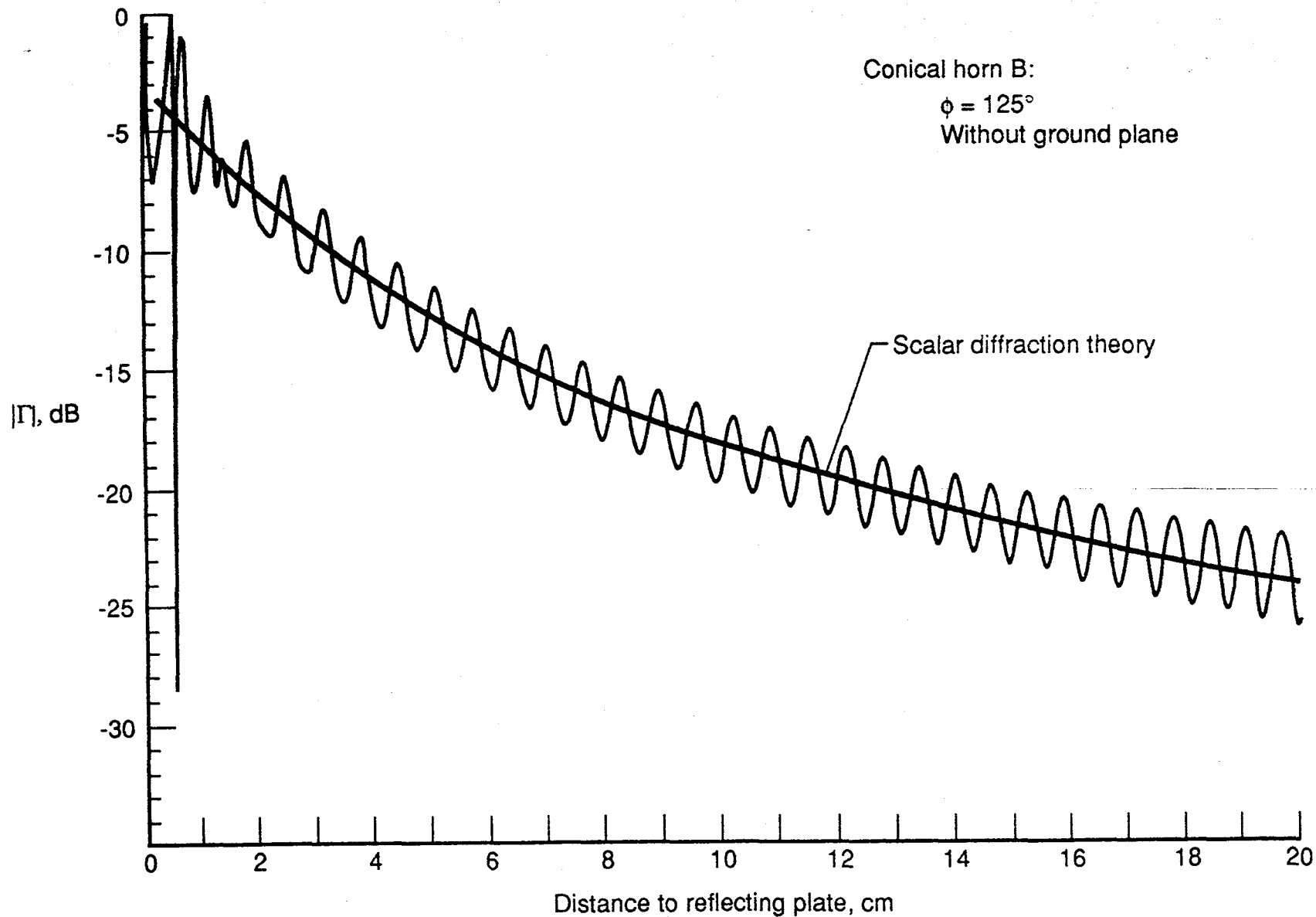


Figure 40. Comparison of scalar diffraction theory predictions with measurements from a 2.54 cm diameter horn.

REPORT DOCUMENTATION PAGE

Form Approved
OMB No. 0704-0188

Public reporting burden for this collection of information is estimated to average 1 hour per response, including the time for reviewing instructions, searching existing data sources, gathering and maintaining the data needed, and completing and reviewing the collection of information. Send comments regarding this burden estimate or any other aspect of this collection of information, including suggestions for reducing this burden, to Washington Headquarters Services, Directorate for Information Operations and Reports, 1215 Jefferson Davis Highway, Suite 1204, Arlington, VA 22202-4302, and to the Office of Management and Budget, Paperwork Reduction Project (0704-0188), Washington, DC 20503.

1. AGENCY USE ONLY (Leave blank)		2. REPORT DATE June 1993	3. REPORT TYPE AND DATES COVERED Technical Memorandum	
4. TITLE AND SUBTITLE 24 GHz Measurements of 2.2 Lambda Conical Horn Antennas Illuminating a Conducting Sheet			5. FUNDING NUMBERS WU 505-64-12-04	
6. AUTHOR(S) A. E. Cross, R. E. Marshall, C. P. Hearn, and R. T. Neece				
7. PERFORMING ORGANIZATION NAME(S) AND ADDRESS(ES) NASA Langley Research Center Hampton, VA 23681-0001			8. PERFORMING ORGANIZATION REPORT NUMBER	
9. SPONSORING / MONITORING AGENCY NAME(S) AND ADDRESS(ES) National Aeronautics and Space Administration Washington DC 20546-0001			10. SPONSORING / MONITORING AGENCY REPORT NUMBER NASA TM-109002	
11. SUPPLEMENTARY NOTES Cross: Research Triangle Institute, Hampton, VA; Marshall: Research Triangle Institute, Hampton, VA; Hearn: Langley Research Center, Hampton, VA; Neece: Langley Research Center, Hampton, VA				
12a. DISTRIBUTION / AVAILABILITY STATEMENT Unclassified-Unlimited Subject Category 32			12b. DISTRIBUTION CODE	
13. ABSTRACT (Maximum 200 words) Monostatic reflection-coefficient magnitude, $ \Gamma $, measurements occurring between a radiating horn and a metal reflecting plate are presented for a family of three 2.2λ diameter conical horn antennas. The three horns have different aperture phase deviations: 6° , 22.5° , and 125° . Measurements of $ \Gamma $ as a function of horn-plate separation (d) extend from an effective antenna aperture short ($d = 0$) to beyond the far-field boundary ($d = 2D^2/\lambda$, where D is the antenna diameter). Measurement data are presented with various physical environments for each of the horns. Measured scalar data are compared with theoretical data from two models, a numerical model for a circular waveguide aperture in a ground plane and a scalar diffraction theory model. This work was conducted in support of the development effort for a spaceborne multifrequency microwave reflectometer designed to accurately determine the distance from a space vehicle's surface to a reflecting plasma boundary. The metal reflecting plate was used in this study to simulate the RF reflectivity of a critically dense plasma. The resulting configuration, a ground plane mounted aperture facing a reflecting plane in close proximity, produces a strong interaction between the ground plane and the reflecting plate, especially at integral half-wavelength separations. The transition coefficient is characterized by large amplitude variations.				
14. SUBJECT TERMS antenna aperture phase deviation, antenna ground plane effects, circular waveguide, millimeter wave measurements, microwave reflectometer, Scalar Diffraction Theory.			15. NUMBER OF PAGES 65	
			16. PRICE CODE A04	
17. SECURITY CLASSIFICATION OF REPORT Unclassified	18. SECURITY CLASSIFICATION OF THIS PAGE Unclassified	19. SECURITY CLASSIFICATION OF ABSTRACT	20. LIMITATION OF ABSTRACT	

